Technical Details of the BRAHMS pp analysis

K. Hagel
Cyclotron Institute, Texas A&M University, College Station, Texas 77843

F. Videbaek
Brookhaven National Laboratory, Upton, New York
(Dated: March 15, 2004)

We present the technical details of the pp analysis.

INTRODUCTION

This report aims to explain the analysis of the p + p data taken at the end of the 2002 RHIC Run. The report presents many of the analysis details focusing on the analysis details which differed from the analysis of the Au+Au data. For example, the timing t_0 used in this run was obtained from the new counters, TD1 (for the FS) and TMrsF (for the MRS). Therefore new calibrations were done and a plots are shown to convince the reader that the calibrations are in order. In addition the vertex was determined using the INEL counters instead of the ZDCs and so there is a discussion regarding the vertex distributions for the different angle/field settings.

This analysis had as the original goal to generate anti-particle/particle ratios with an eventual extension to generate spectra. We therefore focus on the ratios presenting in the end several different ways to look at the ratios and implications.

The report begins with a listing of the assumptions made in this analysis with respect to the analysis of the Au + Au data. We then discuss the additions to the software (brat) to implement the new detectors used in the p+p data. The runs used in the present analysis are listed. The analysis chain used for this analysis is then described. After that there is a discussion on calibrations performed and quality controls. Finally there are two sections dealing with results where the ratios are generated two different ways.

This report concentrates on the data analysis performed at TAMU. To check consistency of the results, Bjorn Samset is performing a parallel analysis in Norway by Bjorn Samset and an analysis report has also been generated. Some of the data in this report are shown as overlays in that report.

ASSUMPTIONS

Several assumptions were made in this analysis. This was basically to take advantage of the significant amount of work done for the Au + Au analysis. Essentially everything was assumed to be "working" unless proven otherwise. In the final results presented here, the assumptions that persisted were the following. The first is that the tracking is taken as having been worked out by "other people" and all of the software works as is. The same was assumed for the RICH pid. There was never a need to question these assumptions through all of the analysis performed.

ENHANCEMENTS TO SOFTWARE (BRAT) FOR PP ANALYSIS

The main enhancement to the software involved adding support for the TD1 and TMrsF counters for the FS and the BFS, respectively. Several modules were added and other modules were modified.

The modules that were added enabled matching of TD1 and TMrsF slats to the respective tracking detectors (T1 for TD1 and TPM1 for TMrsF). These modules were BrTd1MatchingModule and BrTMrsFMatchingModule.

There were three main areas where existing software had to be modified to add new capabilities to deal with the above mentioned data. The first place is in the calibrations, namely the BrTofTimeOffsetCalModule and BrTofSlewingCalModule. The other was in the pid generation module, BrTofPidModule. Two main modifications had to be made. In order to calculate the proper time, T0 had to be calculated using TD1 and TMrsF for the FS and MRS, respectively. This option is activated if the methods SetUseTd1Time(kTRUE) for FS and SetUseMrsTime(kTRUE) for MRS are executed in these modules. The default of fUseTd1Time and fUseMrsTime remain kFALSE by default.

In order to calculate the velocity correctly, the path length of the track had to be calculated from TD1 (TMrsF) to the respective time of flight wall. In order to do that in the FFS, we calculate the distance from TD1 - D1 using BrTd1TrackMatch::GetLength() (which is currently hardwired to 23.5) and the distance from D1 - H1 using BrFfsTrack::GetPartialPath(). In the BFS the distance from TD1 to H2 is calculated by adding the FFS length (TD1-H1) to the distance from H1 to H2 using BrBfsTrack::GetPathLength().

In the MRS, the pathlength of the track is calculated using the distance from TMrsF - TPM1 using BrTMrsFTrackMatch::GetLength() and the distance from TPM1 - TOFW using BrMrsTrack::GetPartialPath().

Another enhancement was a module to estimate the vertex from projections of TPM1 tracks to the center of the beampipe (x = 0). The reason for this is discussed below. A module was developed (BrTrackProjectionVertexModule) which generates a vertex object in this way from a track in TPM1. It is not so different as BrTPMTrackVertexModule, but it allows a vertex object to be built using only one track as an estimate of the vertex. In addition it uses BrDetectorTrack objects from TPM1 instead of the BrTpcTrackCandidate objects that are used by BrTPMTrackVertexModule.

The other enhancement was to add support for Inel vertex filtering as well as TrackProjection vertex filtering in BrVertexFilter. These were added as options which are off by default.

RUNS USED

The runs used in the analysis are shown in table I. These runs gave a y-p_t coverage shown in figure 1. Note that the y-p_t coverage is fairly sharp in this figure. This is because there were cuts applied to the data in order to obtain this figure. The cuts applied will be discussed in a later section. These runs were chosen by selecting runs which had “good” data in both the A and B polarity settings at the particular angles. Inspection of the list will show that there are some angle/field settings which are not optimal. This occurred because of the short run time available. It is felt, however, that there is enough data available to do a ratio analysis.

It should be mentioned that there are a number of fairly high statistics runs where there is a particular angle/field setting for only one polarity. These runs could quite possibly turn out to be useful when extracting spectra and yields in a later part of the analysis. It should be noted that the quality of most of these runs has not been checked.

ANALYSIS CHAIN

The analysis chain was broken into 3 parts. The first part was the local track reconstruction which was performed on the CRS farm. This was done using the bratmain config script brahms_app/kh_app/reco/pp/ProductionReduction.C which is essentially a copy of what was understood to have been used in the Au + Au reconstruction with a few modifications specific to p + p running. This generated output files in the directory $basedir/rxxxx/seq where xxxx is the run number.

The second part used the first part as input and took the local tracks from the different detectors and did the matching. The track-tof matching was done in this stage. The output files were placed in the directory $basedir/rxxxx/gtr. They continued to be separated by seq number at this stage.

The third part was the generation of the DST files. The input was the matched tracks and matched track-tof of the last part as well as the different raw data of other detectors which had been carried along to this stage.

After these three stages, the dst files could be used for physics analysis. Several scripts and modules were written to utilize these dst files.

CALIBRATIONS

The only detectors that were calibrated by us for the present analysis were the new timing detectors (TD1 and TMrsF), the time of flight detectors and pp2pp timing slats (INEL) which were used for the vertex determination and minimum bias trigger. All other detector were either calibrated by other collaborators and put into the calibration DB for transparent use or the latest calibrations from the Au + Au run were used.

The calibrations that were done for the time of flight walls mainly involved extracting new offsets taking into account the fact that TD1 and TMrsF are now being used to calculate T0. Slewing correction calibrations were also performed. This involved a modification to the software as explained above for pid module. Calibrations also had to be performed on H1, H2 and TOFW. The runs used for the various calibrations are shown in table II.

QUALITY CONTROL

Calibrations

In order to judge whether the new TOF calibrations reached the performace specifications of the detectors, they were checked by looking at the time difference between each slat and the TD1 or TMrsF detectors. Figure 2 shows the distributions of this time difference for different slats in H2.

The actual numbers for each slat are shown in table III. To get the slat resolution, a resolution of 60 ps was assumed for TD1. That this assumption for TD1 was reasonable was later verified by tests which compared the different slats of TD1 to each other. The results were found to be dependent on run, but in general 60 ps was found to be reasonable.

Vertex Distributions

Beam delivery from RHIC during the pp run sometimes gave unexpected results. This was noticed online by monitoring the vertex distribution obtained from the

TABLE I: Runs used for different spectrometer settings

Angle	D1 (D5) current	runs
90	1050A	6714,6715,6722,6723
90	1000B	6669,6673,6674,6675,6676,6677,6682,6689,6690,6691
90	1000B	6703,6740,6741,6748,6750,6751,6752,6753,6754
90	350A	6706,6707,6713
90	344B	6251,6256,6257,6630,6631,6633,6636,6637,6638,6639
60	500A	6433,6434,6435
60	500B	6442,6443,6444,6445,6446,6447,6448,6449
45	700A	6415,6417,6418,6419,6420,6427,6428,6429,6431,6432
45	700B	6401,6405,6410,6411
40	700A	6318,6319,6320,6321,6322
40	700B	6331,6345,6346,6374,6375,6394,6398,6399,6400
35	700A	6303,6313,6314,6315,6316
35	700B	6270,6271,6277,6278,6279,6289,6300,6302
20	230A	6445,6446,6447.6448,6449
20	230B	6445,6446,6447.6448,6449
12	843A	6257,6277,6289,6278,6279
12	843B	6398,6399,6400,6401,6405,6410,6411
4	1124A	6418
4	1124B	6428,6429,6431,6432
3	1124A	6473,6488,6493
3	1124B	6669

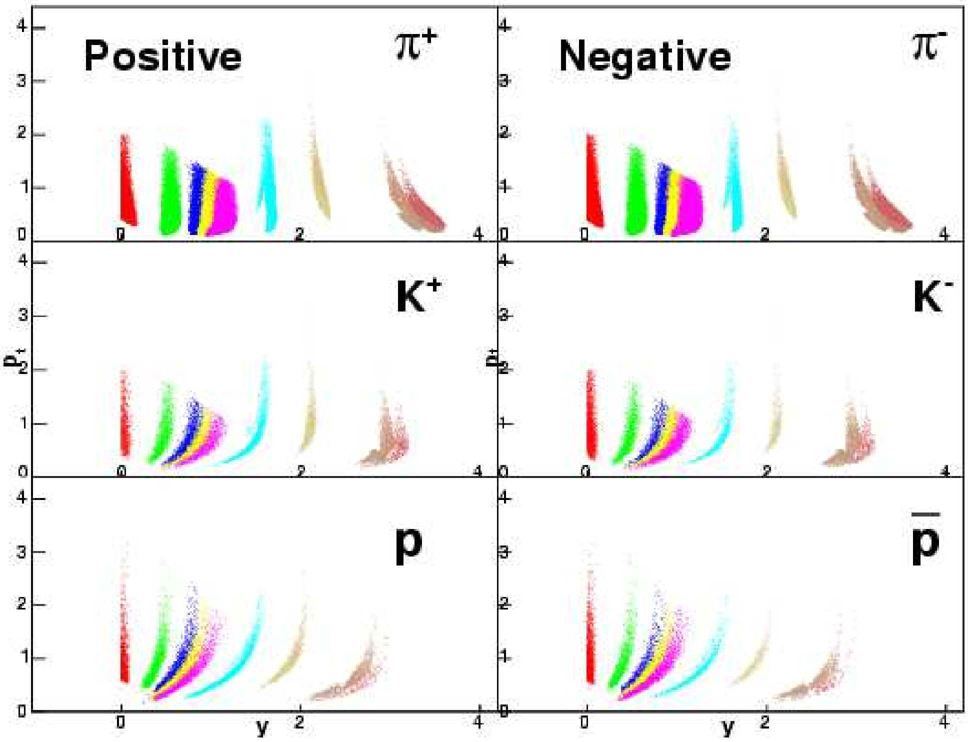

FIG. 1: y-p_t coverage of runs analyzed

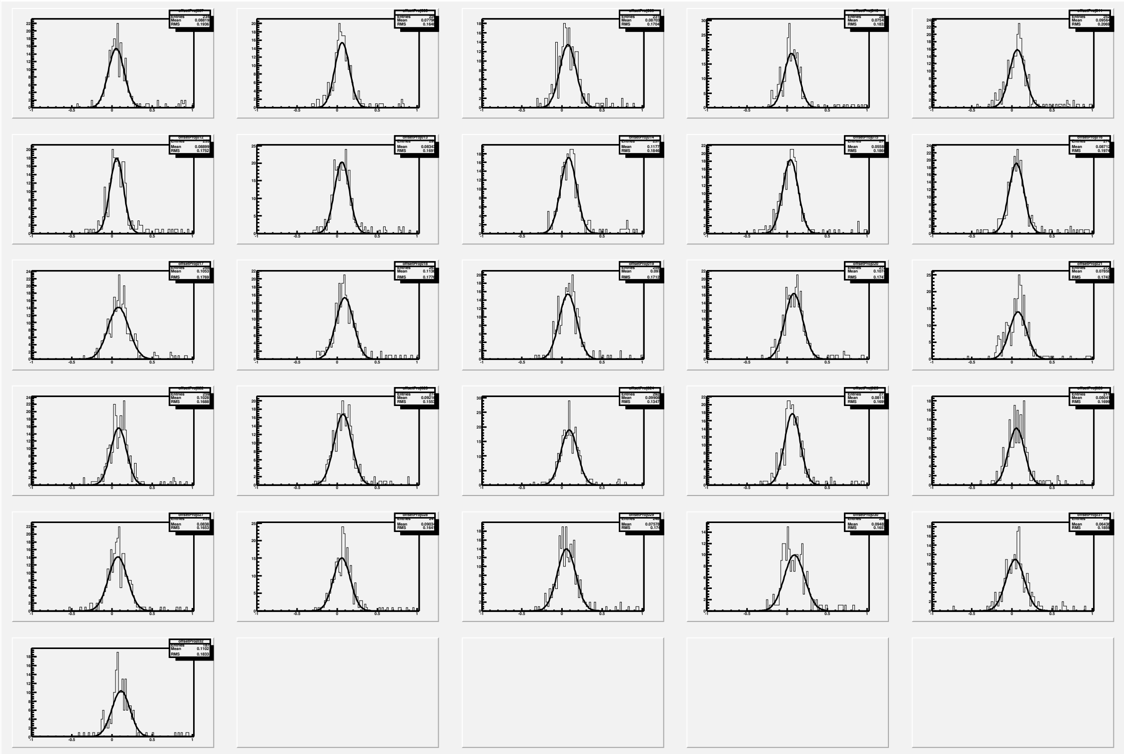

FIG. 2: TOF2-TD1 time difference after new calibration applied

TABLE II: Runs used for calibrating various detectors

Detector	offset	slewing
H1	6383,6418,6473	6383,6473
H2	6383,6418,6473	6383,6473
TOFW	6278,6315,6318,6394,6405,6418	6278
INEL Vtx	6257,6278,6279,6315,6434,6435,	
INEL Vtx	6442,6443,6446,6449,6627,6628	

INEL counters. It has been determined that it is necessary to control carefully the range of vertices allowed for the analysis. In the following we show the accepted vertex distributions for both min bias events as well as for events which had a track for the runs under consideration. Figures 3 and 4 show the vertex distribution for the FS at 3^o and 4^o, respectively, with a field setting of 1124 amps and figure 5 shows the vertex distribution for the FS at 12^o and field setting of 843 amps. Figures, 7, 8, 9, 10, 11 and 12 show the vertex distributions for the MRS at 90^o (D5=1000), 90^o (D5=300), 60^o (D5=500), 45^o (D5=700), 40^o (D5=700) and 35^o (D5=700), respectively. It is seen in all of these plots that there is experimental acceptance over the full range of min bias events.

Finally figure 13 shows the normalized vertex distributions for both minimum bias events as well as events with tracks for all runs added together for each angle/field setting. The minimum bias events are normalized which defines the area under the minimum bias curve to be unity. The distributions with tracks were scaled by 1000 in order to have them on a reasonable scale. The minimum bias distributions are shown as dashed blue and the distributions associated with tracks are represented by solid red lines. Both the A and B magnet polarity settings are overlayed on each plot.

We can see in figure 13 that we have acceptance for tracks over the entire vertex distribution. The shape of the distributions changes somewhat in that the minimum bias distributions display a peak (usually off 0) whereas the distributions associated with tracks reveal a rather flat distribution. The only exception to this is the FS 12^o setting, but even here there are events over the entire vertex range.

It is also possible to derive the vertex from MRS tracks projected to the beam axis. To do that we constructed another module named BrTrackProjectionVertexModule which projects MRS tracks back to the beam axis and constructs a vertex object. In addition, BrVertexFilter was modified to allow vertices determined in this way to be filtered. In order to make things general and be able to use for the forward spectrometer as well (where there were very few MRS coincidences) a pp collision filter module was written (BrPpCollisionFilter) This module can filter on Inel vertices as well as Track Projection vertices depending on how options are set. If *either* vertex lies within the specified limits (they can be specified

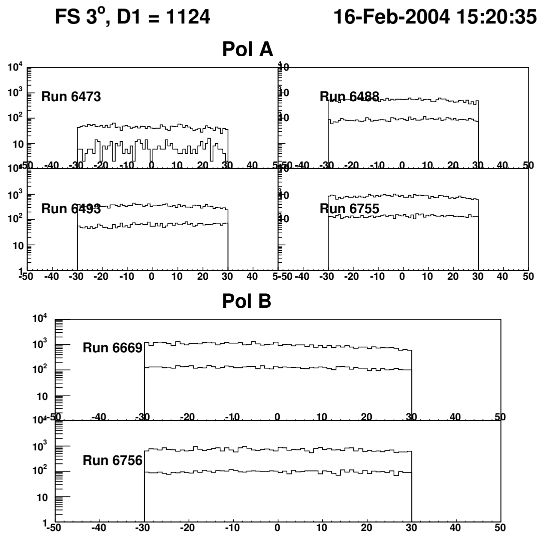

FIG. 3: Inel vertex dist for runs with FS at 3^o and field of 1124 amps

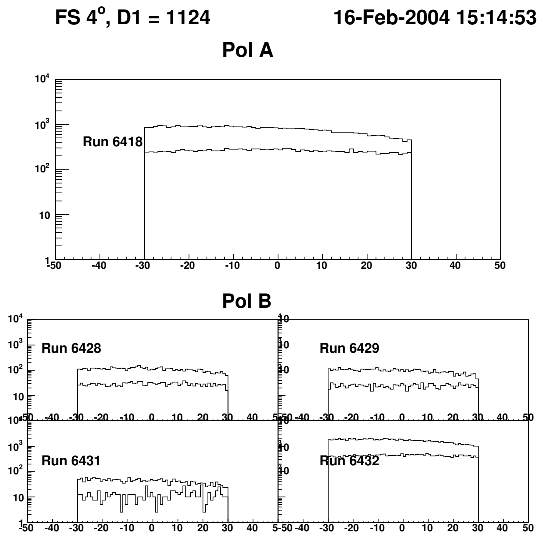

FIG. 4: Inel vertex dist for runs with FS at 4^o and field of 1124 amps

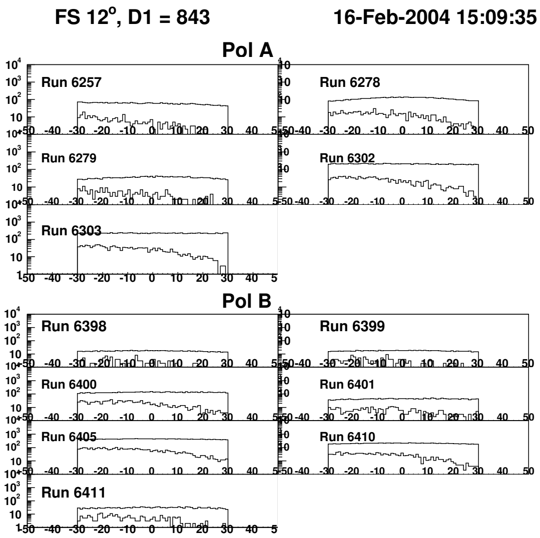

FIG. 5: Inel vertex dist for runs with FS at 12^o and field of 843 amps

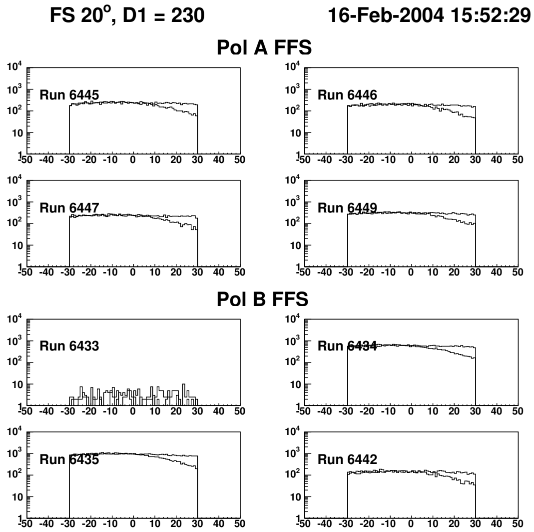

FIG. 6: Inel vertex dist for runs with FFS at 20^o and field of 230 amps

Slat	Overall σ (ns)	slat σ (ps)
7	0.0998263	79.7828
8	0.0913676	68.9061
9	0.101334	81.6617
10	0.0928216	70.8226
11	0.0988938	78.6129
12	0.0853685	60.727
13	0.0932114	71.3328
14	0.100275	80.344
15	0.0964351	75.4966
16	0.0945879	73.1224
17	0.129925	115.241
18	0.11015	92.3743
19	0.11036	92.6246
20	0.111753	94.2795
21	0.107698	89.4358
22	0.0989942	78.7391
23	0.110264	92.5102
24	0.103421	84.237
25	0.0985714	78.2069
26	0.101083	81.3492
27	0.119423	103.256
28	0.105501	86.7786
29	0.11442	97.4265
30	0.126748	111.647
31	0.115671	98.8927
32	0.112317	94.9474

TABLE III: TOF2 slat timing resolution after slewing. The middle column shows the overall resolution and the right column shows the slat resolution with an assumed resolution of 60 ps in TD1.

independently), the event is accepted.

To see if we can trust generating the vertex in this way, we plot the determined Inel vertex vs the determined track projection vertex in a run where the Inel vertex had coincidences with matched tracks. This is shown in figure 14. We observe in the figure that for this particular run that for Inel vertices $-40 < z < 40$, the distribution is linear, but fairly wide. However, in run 6315 there was a component in the inel vertex at -70 cm which gave a reasonable distribution of TPM1 vertices. If this is in fact happening in runs where we do not observe such a correlation, we will have no way of knowing if we just take a projection on the y axis (use TPM1 track projection as vertex)

The project of deriving the vertex from MRS tracks was begun because of a perceived problem in the vertex in a number of ranges of runs. In fact, that problem was eventually traced to another source and the MRS track projection vertices were never used in the present analysis. Nevertheless, it is usefull to see that it can be done and if necessary the MRS track projection can give a hint on the vertex resolution.

In figure 15 we show the vertex distribution accepted by this scheme. It should be noted that if there are no Inel that we cut the upper and lower parts all the way across the Inel distribution (x axis) instead of allowing as we do in this run the Proj events that happen to be inside the Inel window.

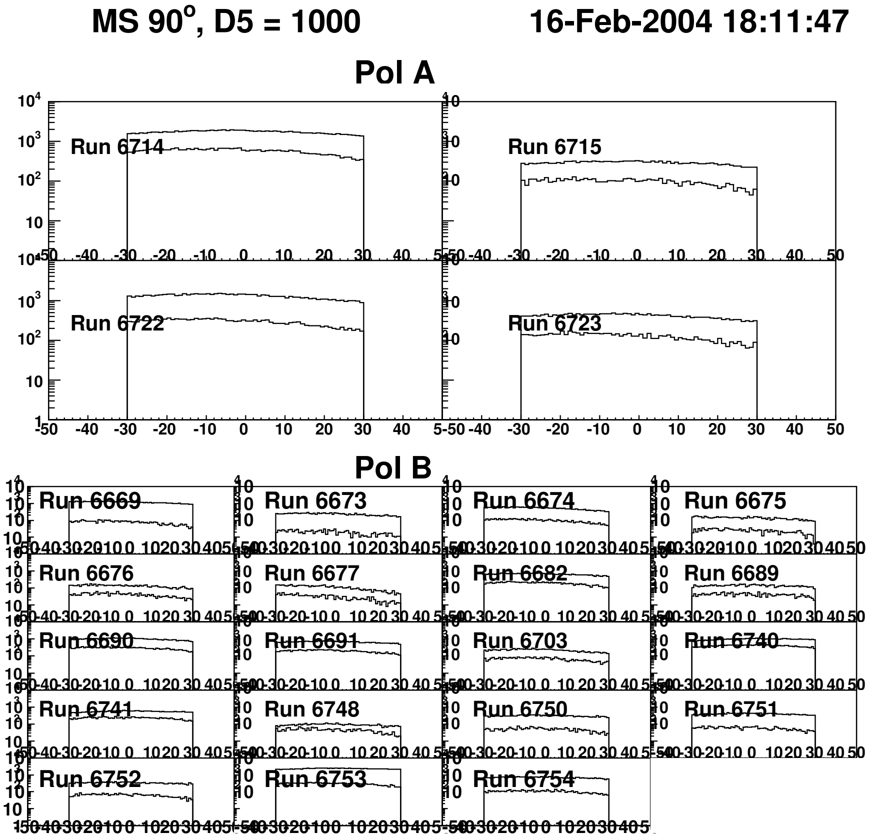

FIG. 7: Inel vertex dist for runs with MRS at 90^o and field of 1000 amps

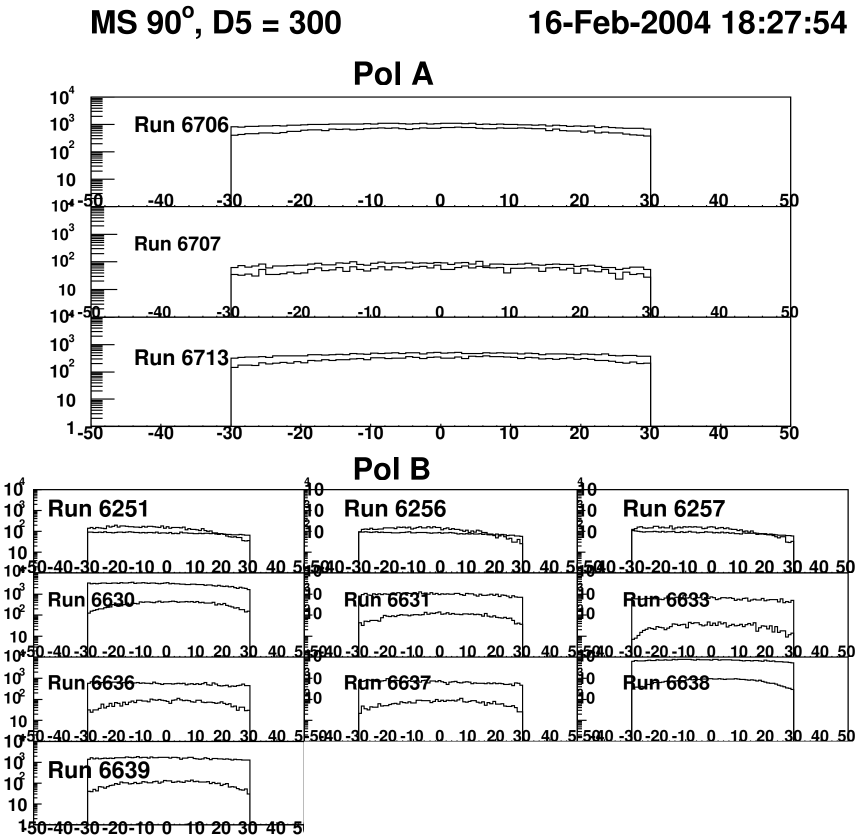

FIG. 8: Inel vertex dist for runs with MRS at 90^o and field of 350 amps

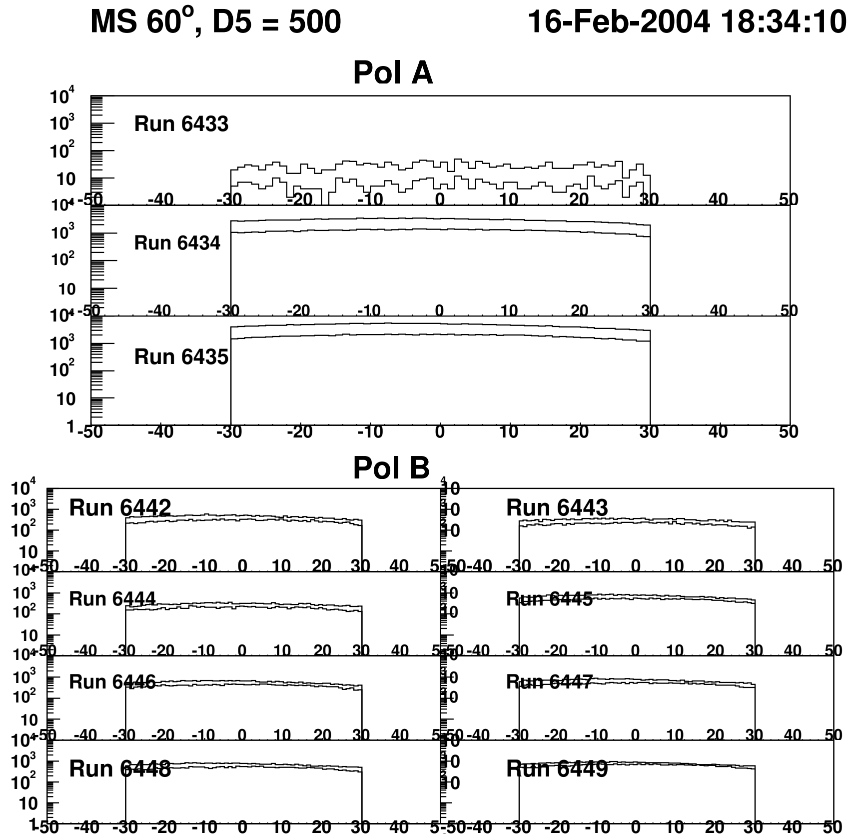

FIG. 9: Inel vertex dist for runs with MRS at 60^o and field of 500 amps

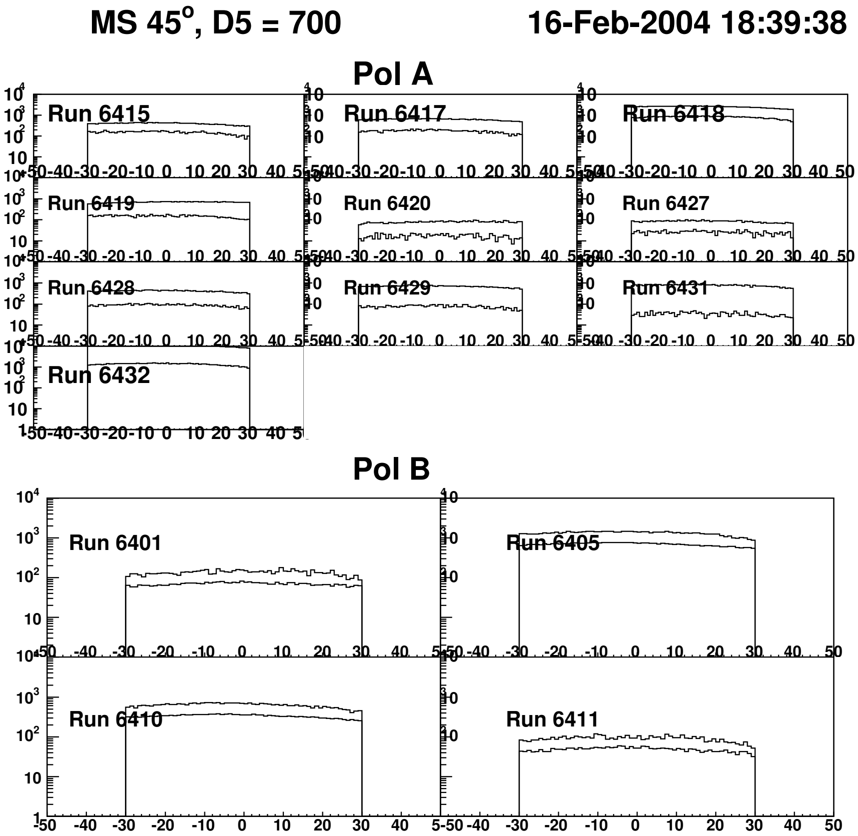

FIG. 10: Inel vertex dist for runs with MRS at 45^o and field of 700 amps

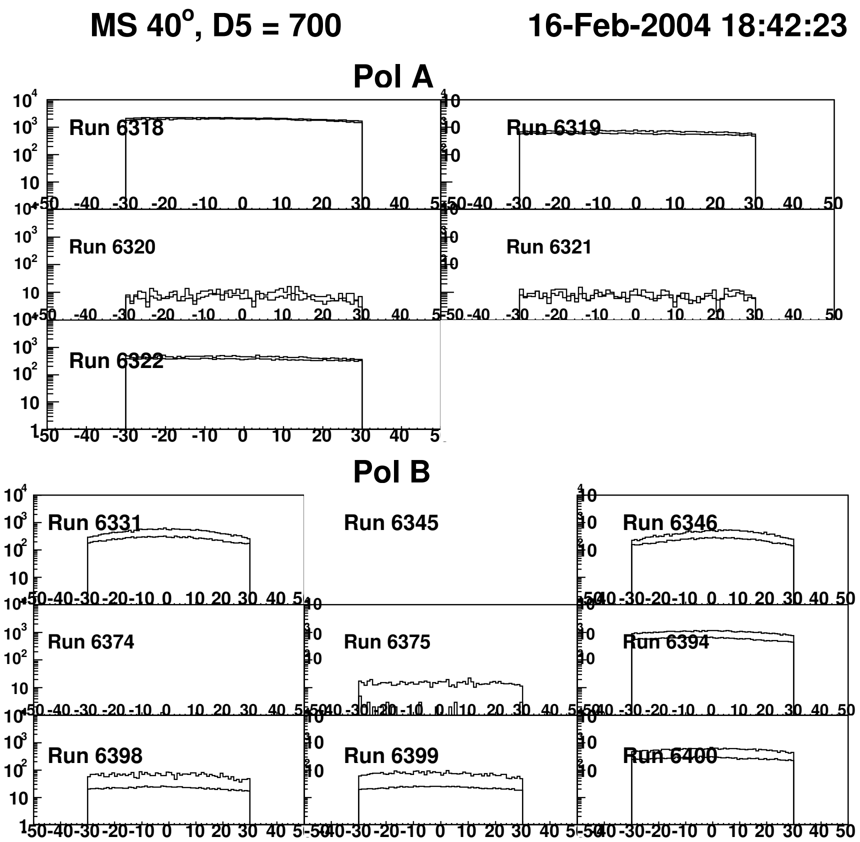

FIG. 11: Inel vertex dist for runs with MRS at 40^o and field of 700 amps

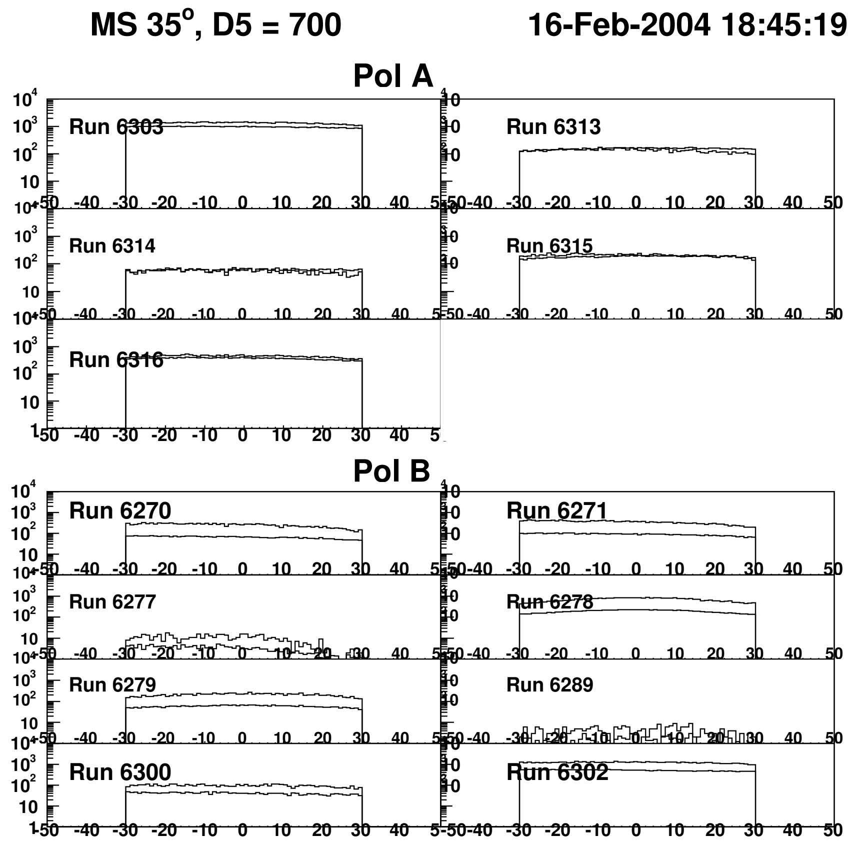

FIG. 12: Inel vertex dist for runs with MRS at 35^o and field of 700 amps

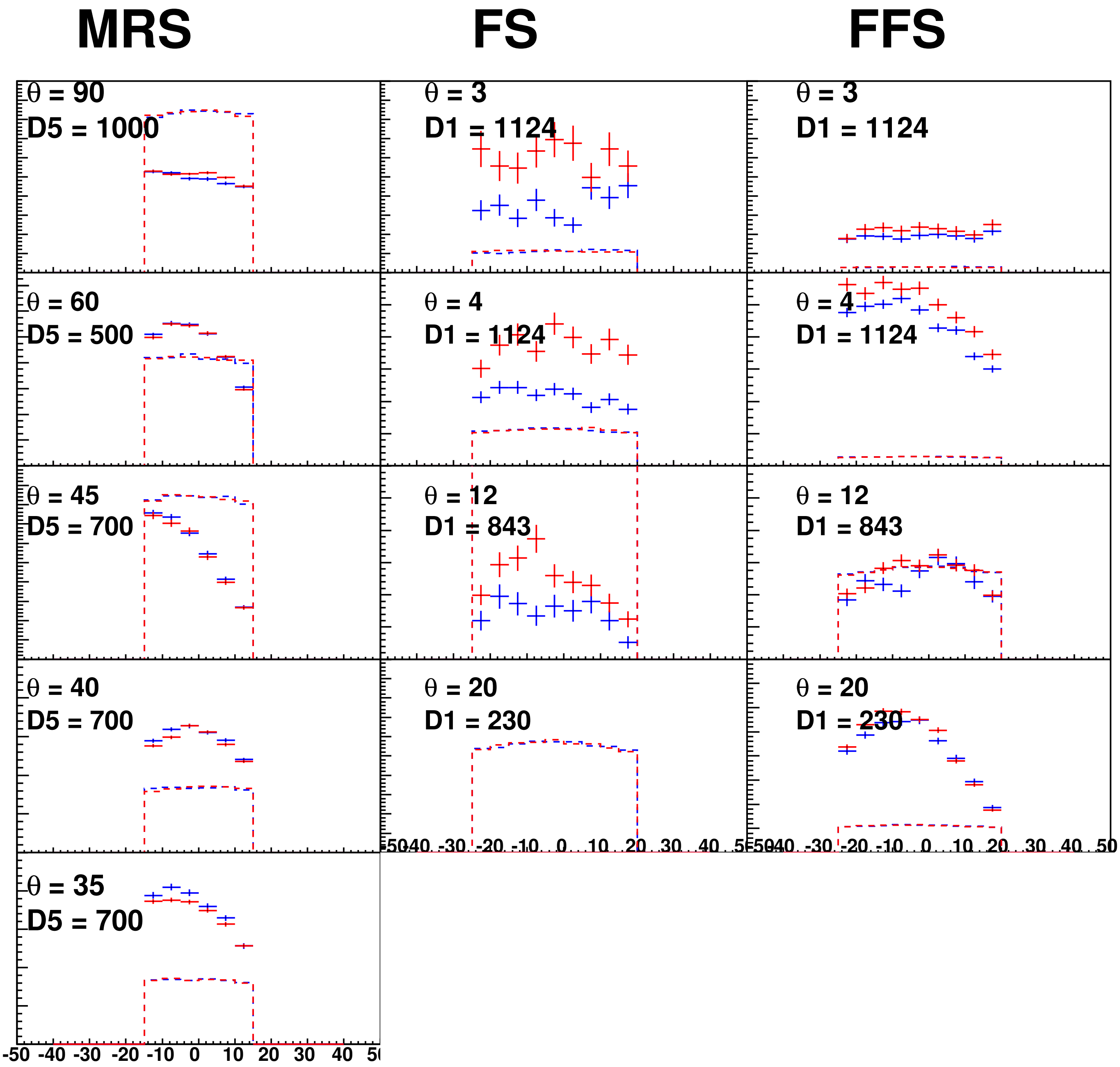

FIG. 13: Inel vertex distributions

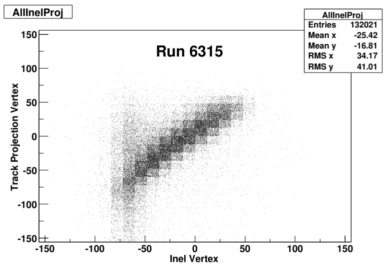

FIG. 14: Inel vs track projection vtx run 6315 (where both appeared to be working)

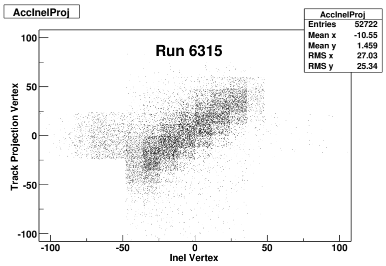

FIG. 15: Accepted Inel vs track projection vtx run 6315 (where both appeared to be working)

Particle Identification

In this section we present the m^2 vs p plots for the runs used in the analysis. Different techniques are used to exploit the BRAHMS particle identification capabilities.

Forward Spectrometer

Figures 16 through 21 show the m^2 vs p plots when the FS was placed at 3^o with D1 = 1124 (1/3 full field). The lines and curves show the boundaries of particle identification for the different combinations of detectors that fired (or did not fire). The different plots show the contributions from events where C1 did not fire and the particle had p less than the pion threshold (NoC1Low), where C1 did not fire and the particle had p greater than the pion threshold (NoC1High) and where C1 did fire (WithC1). In the same way the BFS spectra were constructed by adding together the pid'd contributions from events where RICH did not fire and the particle had p less than the pion threshold (NoRichLow), where RICH did not fire and the particle had p greater than the pion threshold (NoRichHigh) and where RICH did fire (WithRich).

Figures 22 through 27 show the same plots for the 4^o (D1=1124; 1/3 full field) setting.

Figures 28 through 33 show the same plots for the 12^o (D1=843; 1/4 full field). In these plots we can observe that the TOF arrays become more important in determining PID because there are more events when C1 and/or RICH did not fire. This is a result of the lower momentum at this larger angle and relatively low field setting.

Finally 34 through 36 show the same plots for the 20^o setting. There is no BFS information here because the BFS cannot be moved to 20^o. We note, however, very good pid using the FFS.

Mid-rapidity Spectrometer

Figures 37 through 42 show the m^2 vs p plots for the MRS at angles of 35^o (D5=700), 40^o (D5=700), 45^o (D5=700), 60^o (D5=500), 90^o (D5=300) and 90^o (D5=1000), respectively. The different lines show the boundaries of the particle identification. These plots show the accepted particles, so there are no particles shown outside the lines. The πs and Ks are cut at p = 2.0GeV/c. The mean of each particle group was taken between the valleys of each particle species. The center of the upper and lower limits of the pid curves were then set to this mean on a run by run basis.

RESULTS

The DST files were read to produce p_t spectra. These p_t spectra had the cuts shown in table IV applied. After the cuts were applied, π, K, p p_t spectra were accumulated in individual spectra.

TABLE IV: Cuts applied to the data

cut	value
Vertex Cut	-10 - 10
Trigger Cut	(MRS or FS; 3 or 6)
Track Vertex Cut	2σ
Detector Fiducial Cut	
Magnet Swim Status Cut	
Pid Cut	p dependent curves for 2σ cut
Rapidity Cut	depending upon particle

The spectra were incremented event by event and were normalized at the end of event reading. The FS spectra were normalized by a factor of

$$scaleTrig6/(numInel * scaleTrig5)$$

and the MRS spectra were normalized by a factor of

$$scaleTrig6/(numInel * scaleTrig5)$$

where numInel is the number of inelastic events (trig 5) with a vertex inside the limit of ±40cm. Projections were made on each of the axes of the 3D spectra in order to check the data for consistency.

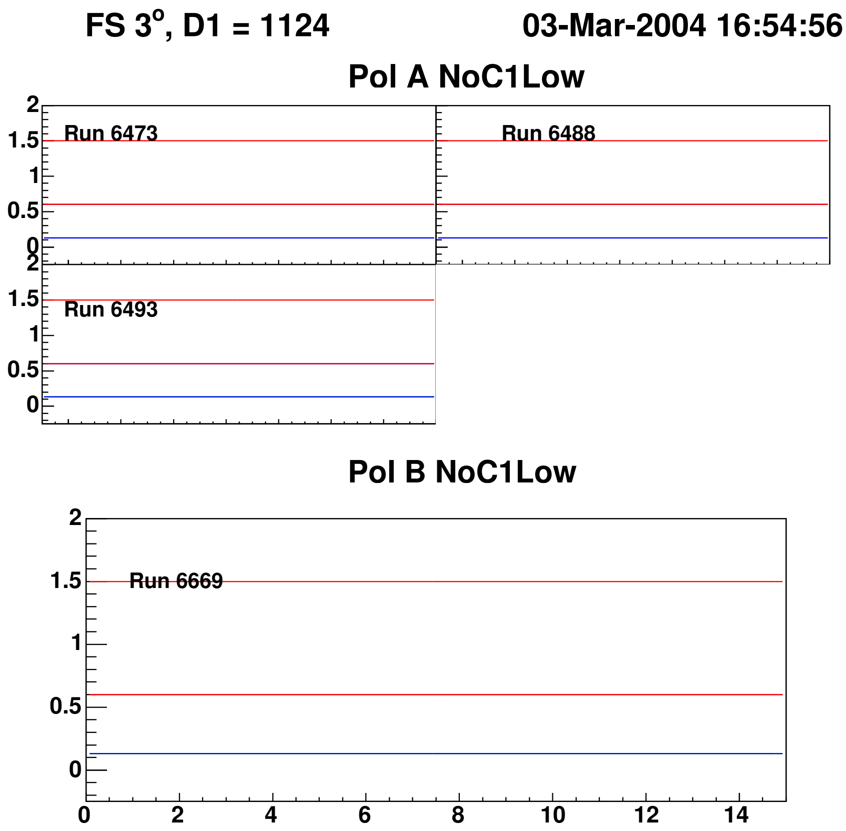

FIG. 16: 3^{o} FFS m^2 vs p (D1=1124)

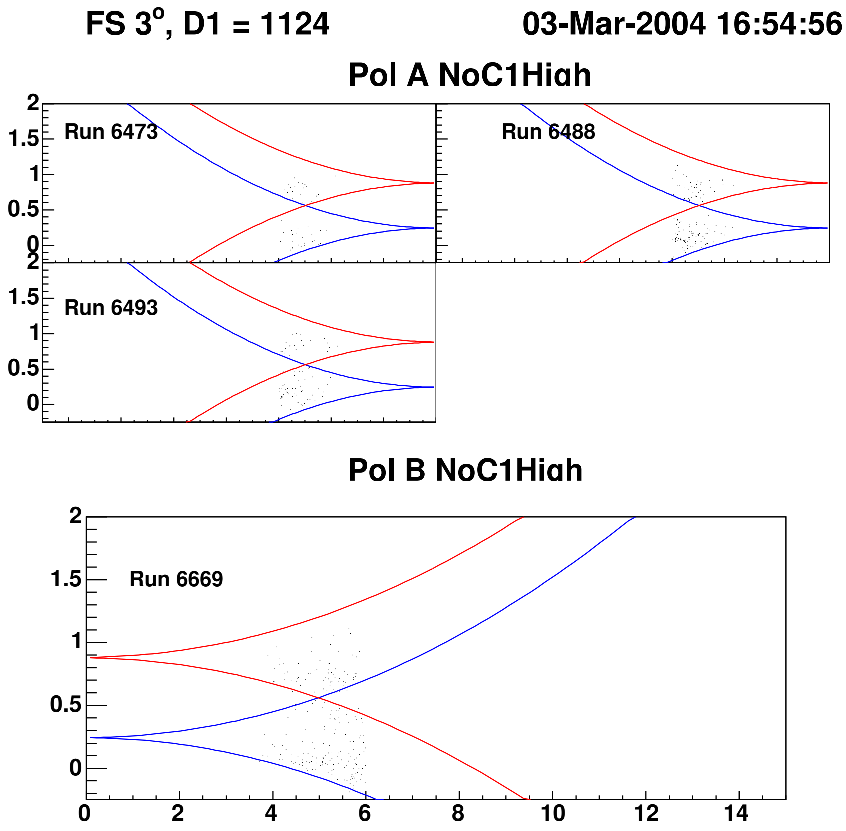

FIG. 17: 3^{o} BFS m^2 vs p (D1=1124)

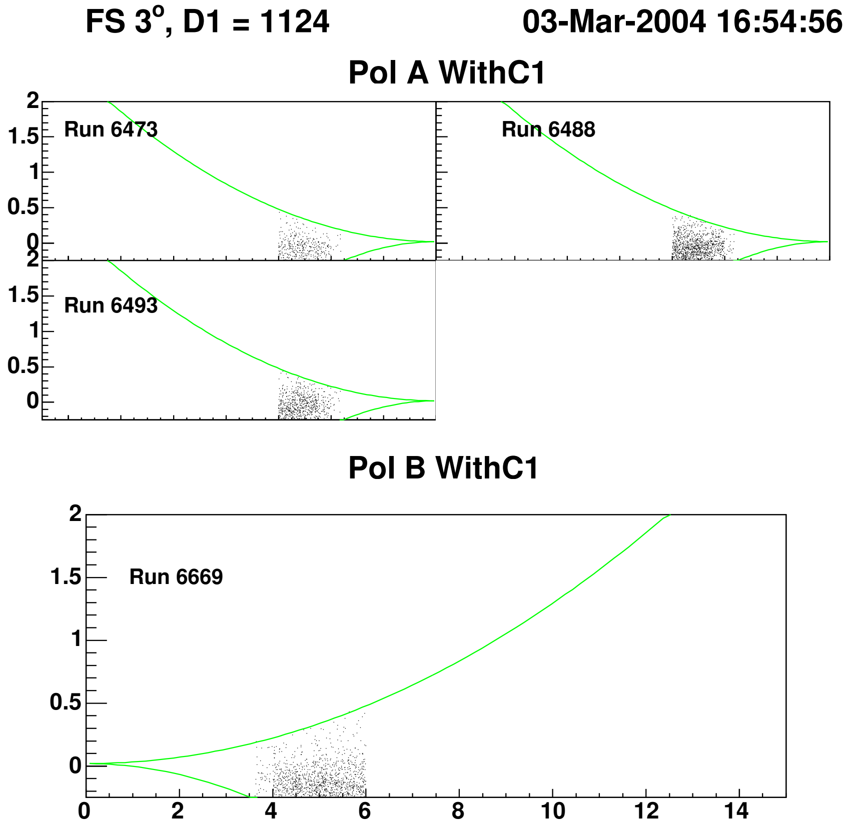

FIG. 18: 3^o BFS m^2 vs p (D1=1124)

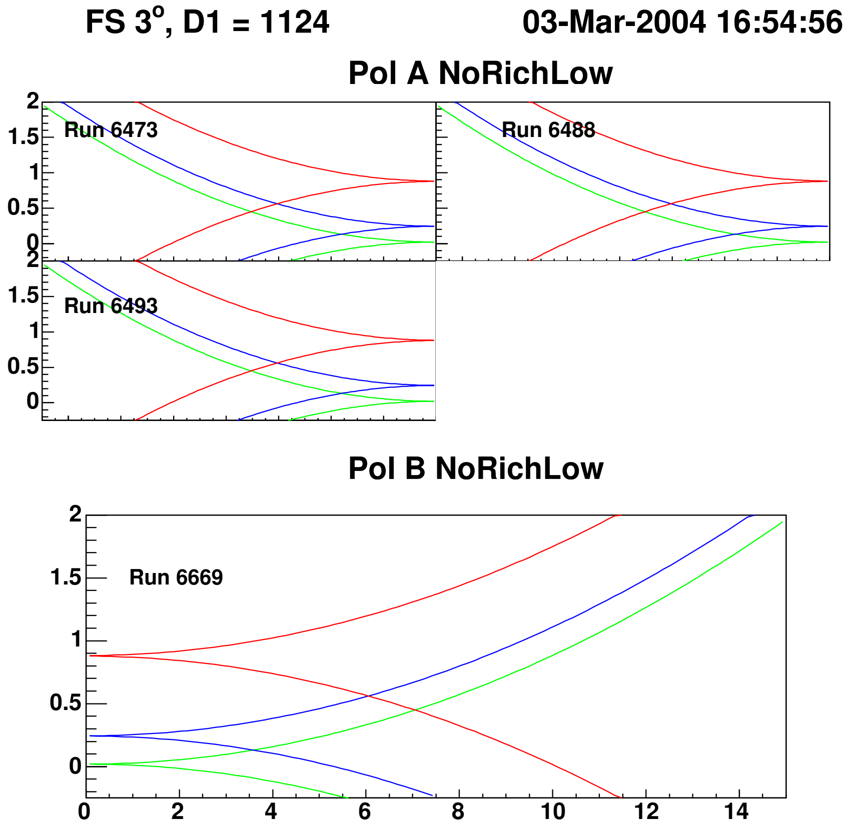

FIG. 19: 3^o FFS m^2 vs p (D1=1124)

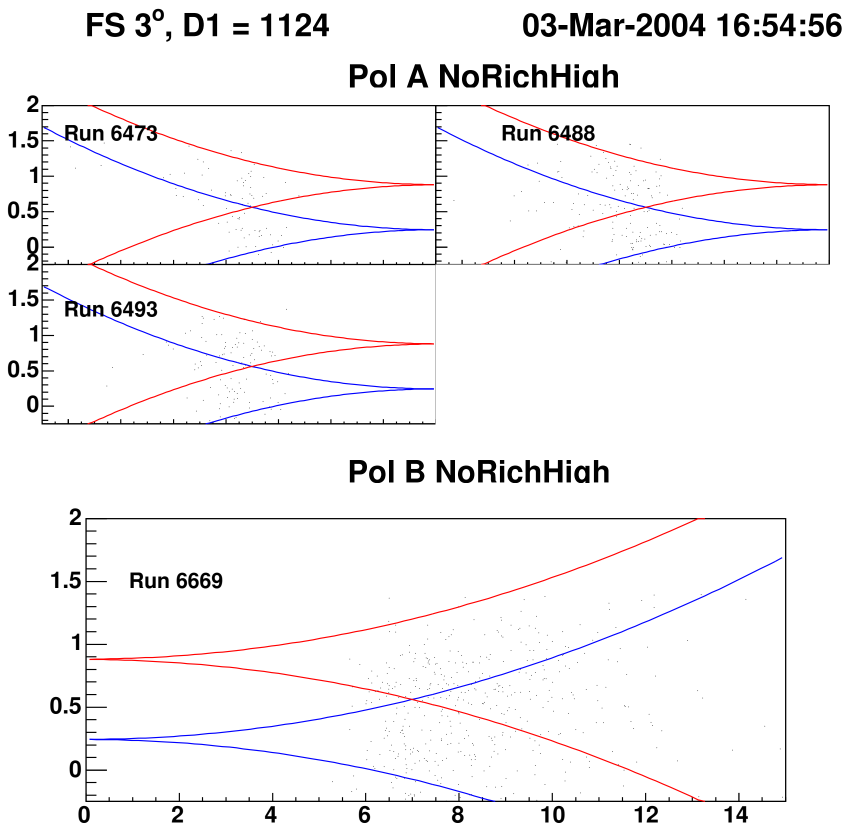

FIG. 20: 3^o BFS m^2 vs p (D1=1124)

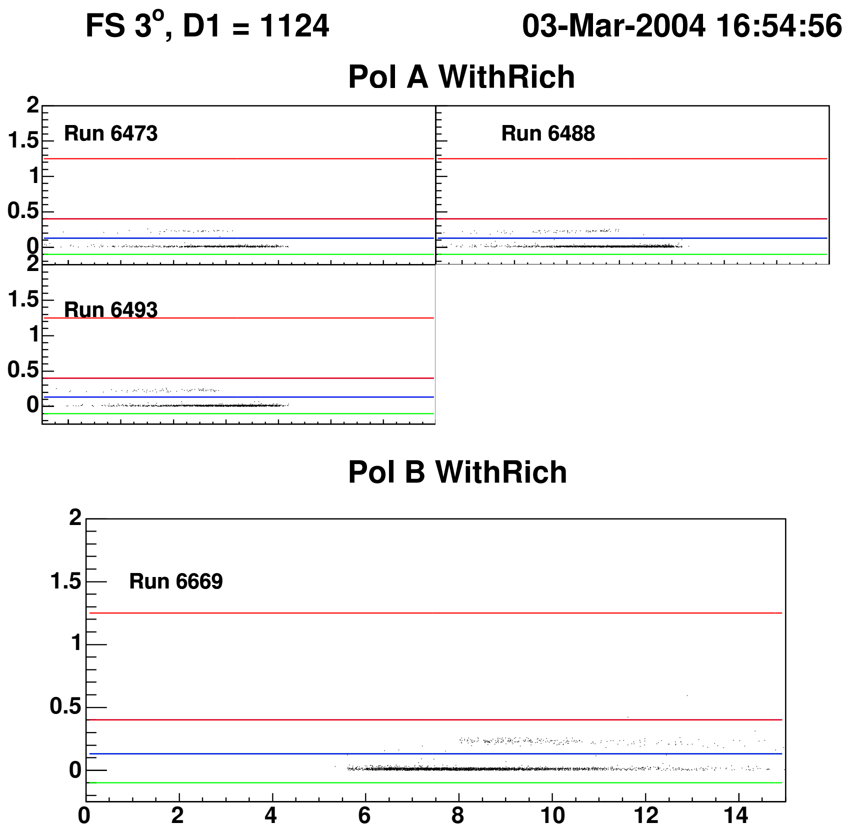

FIG. 21: 3^o BFS m^2 vs p (D1=1124)

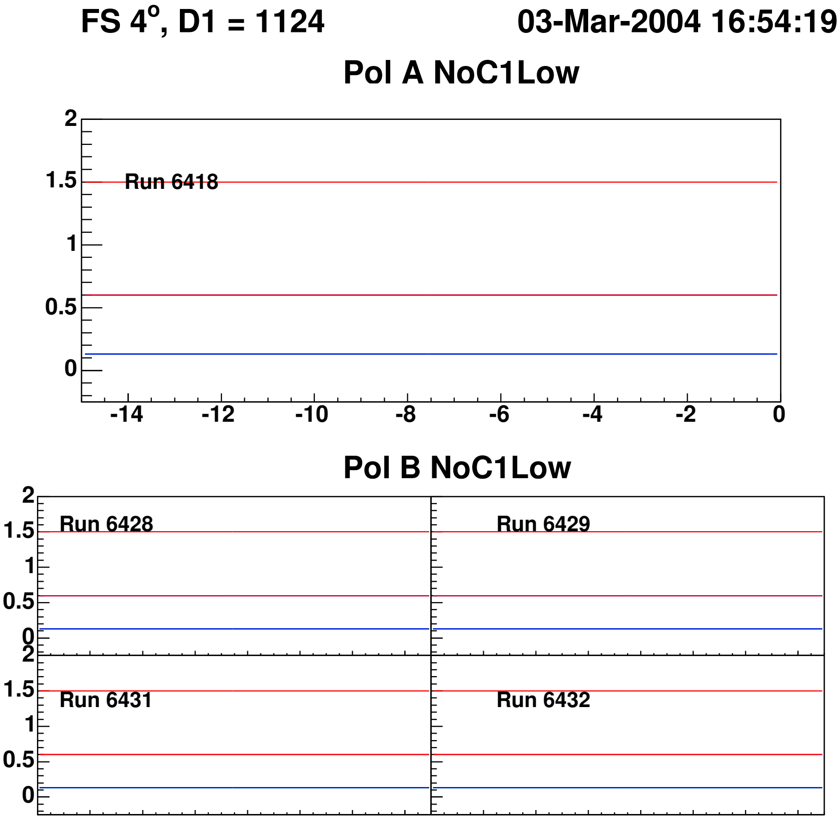

FIG. 22: 4^o FFS m^2 vs p (D1=1124)

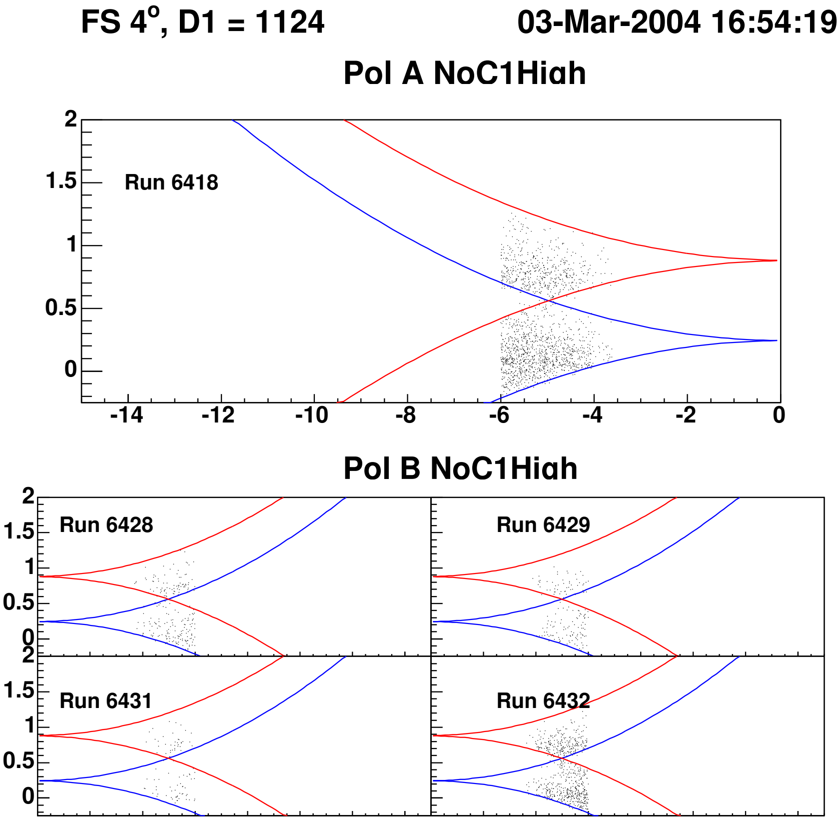

FIG. 23: 4^o BFS m^2 vs p (D1=1124)

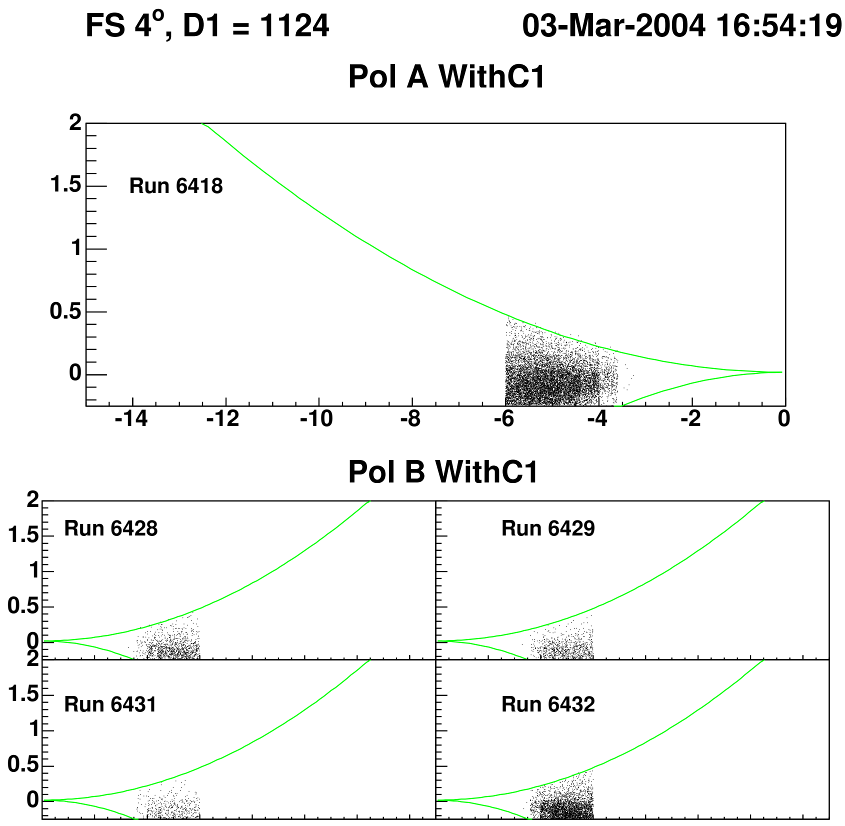

FIG. 24: 4^o BFS m^2 vs p (D1=1124)

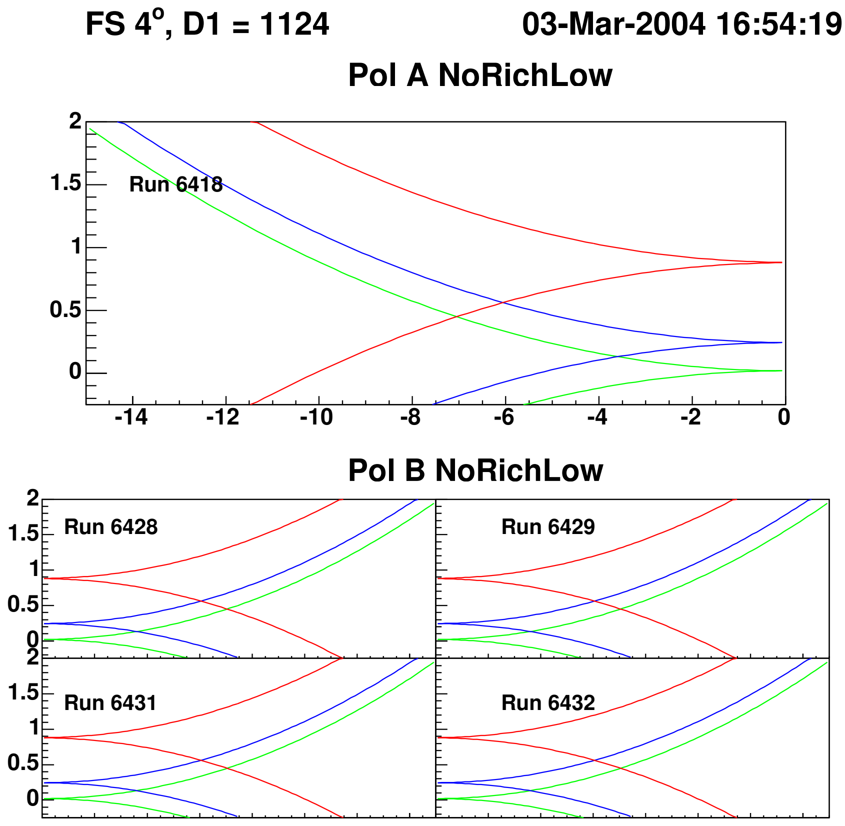

FIG. 25: 4^o FFS m^2 vs p (D1=1124)

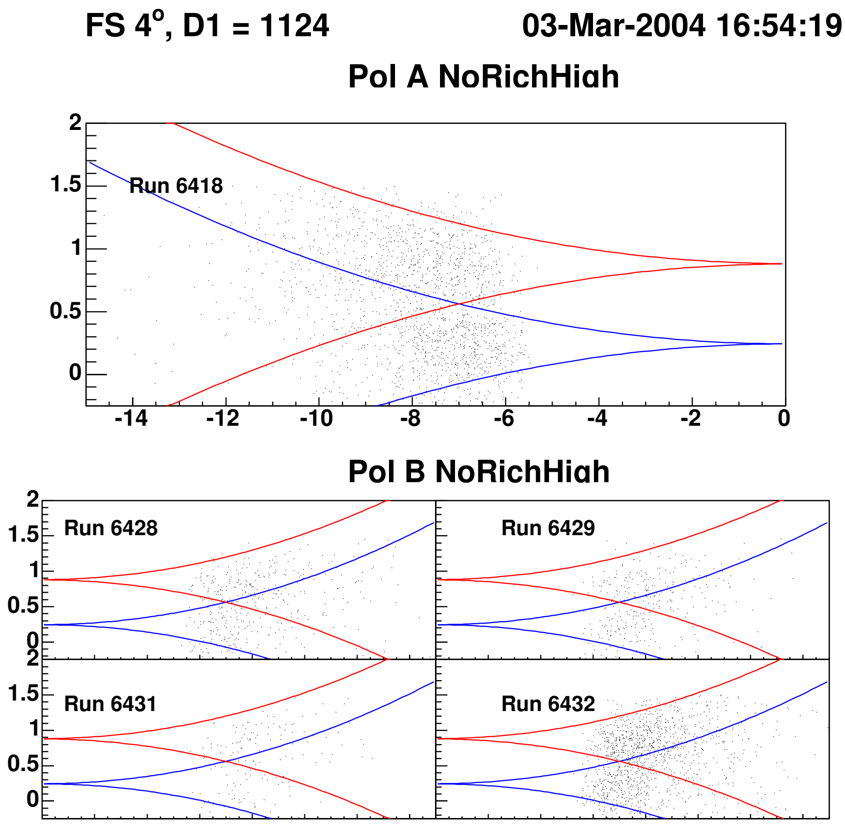

FIG. 26: 4^o BFS m^2 vs p (D1=1124)

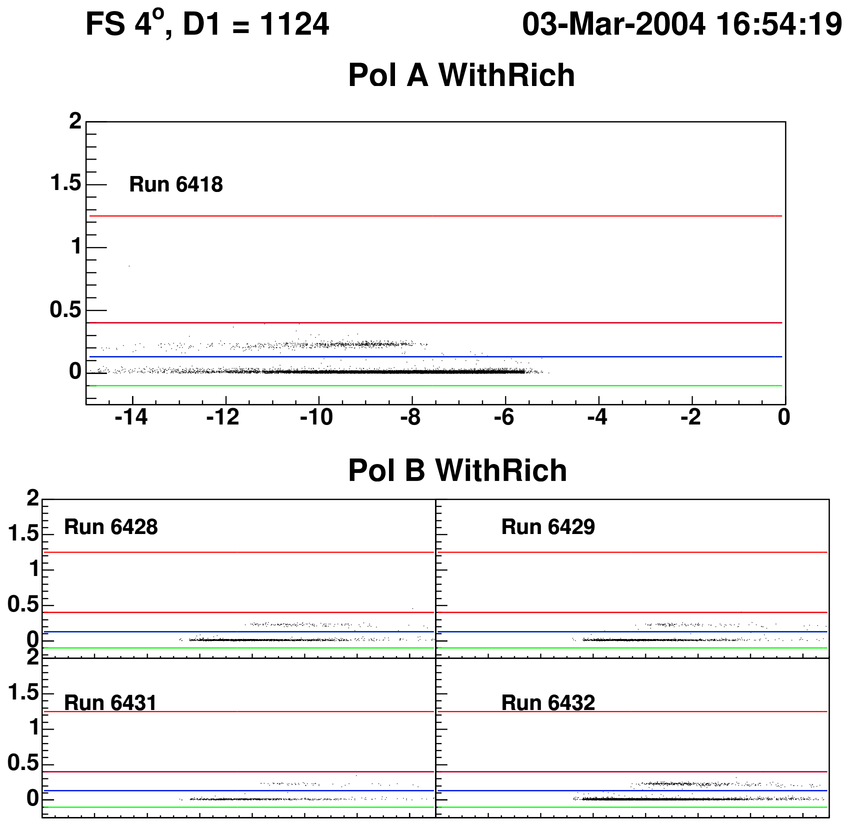

FIG. 27: 4^o BFS m^2 vs p (D1=1124)

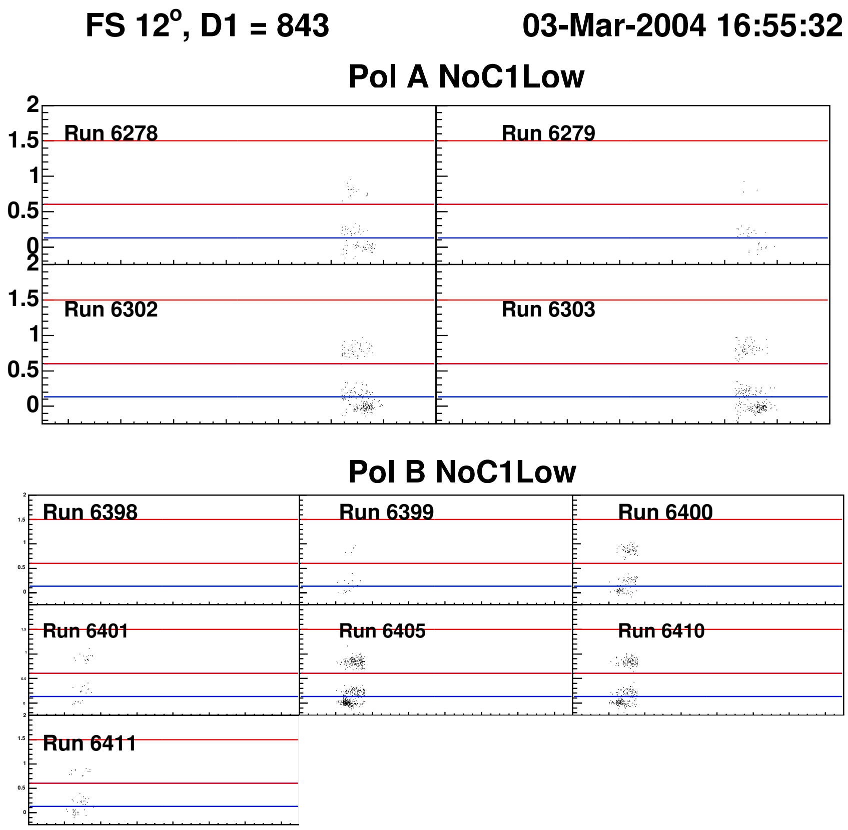

FIG. 28: 12^o FFS m^2 vs p (D1=843)

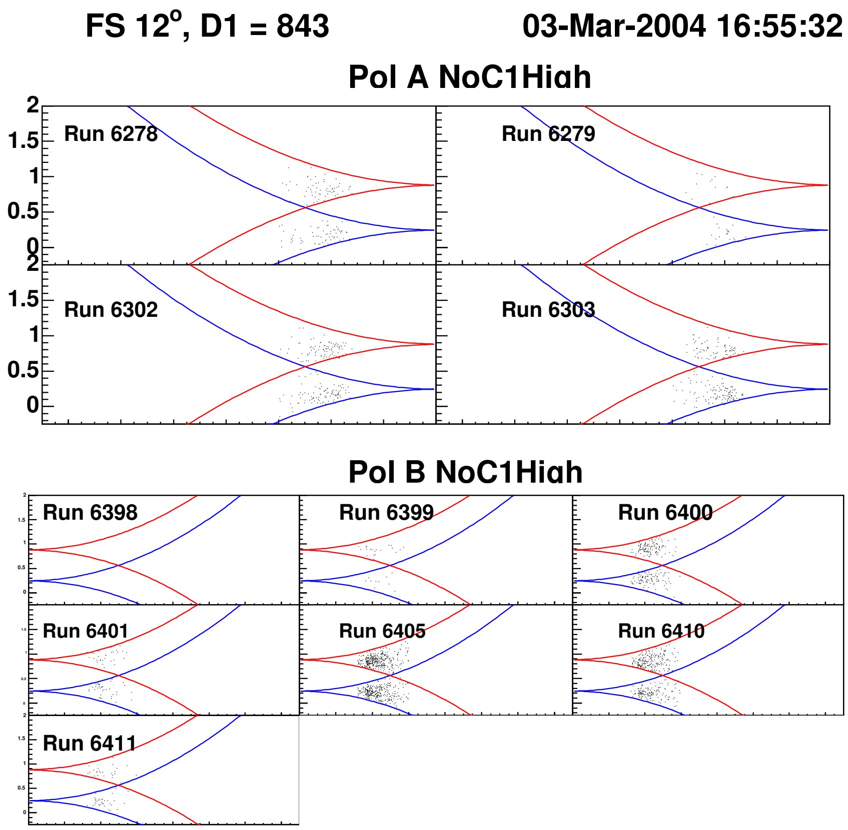

FIG. 29: 12^o BFS m^2 vs p (D1=843)

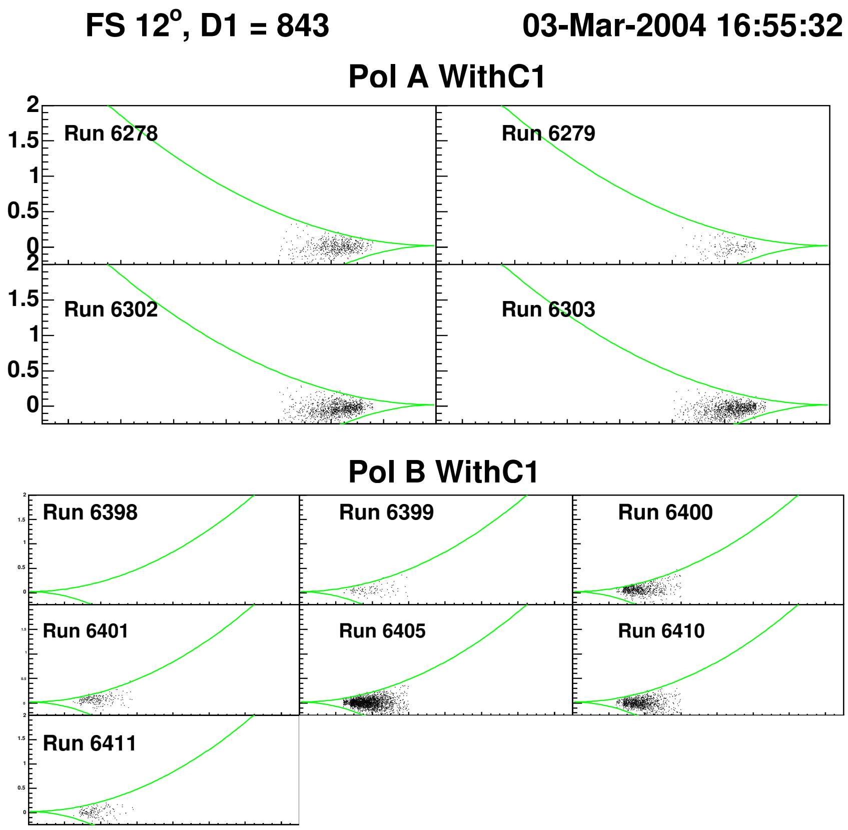

FIG. 30: 12^o BFS m^2 vs p (D1=843)

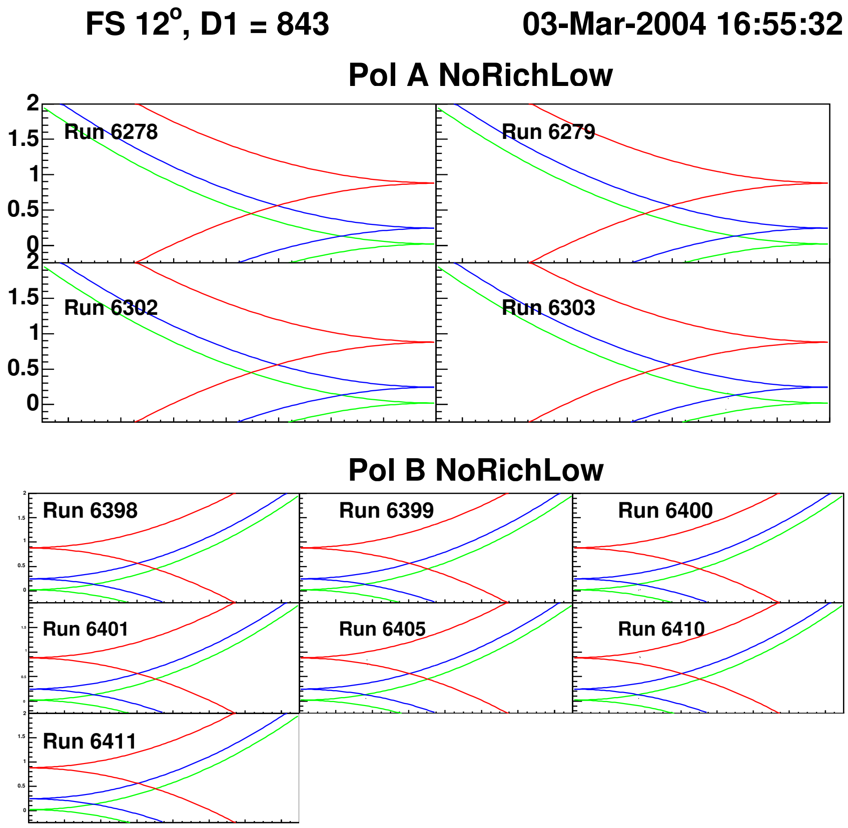

FIG. 31: 12^o FFS m^2 vs p (D1=843)

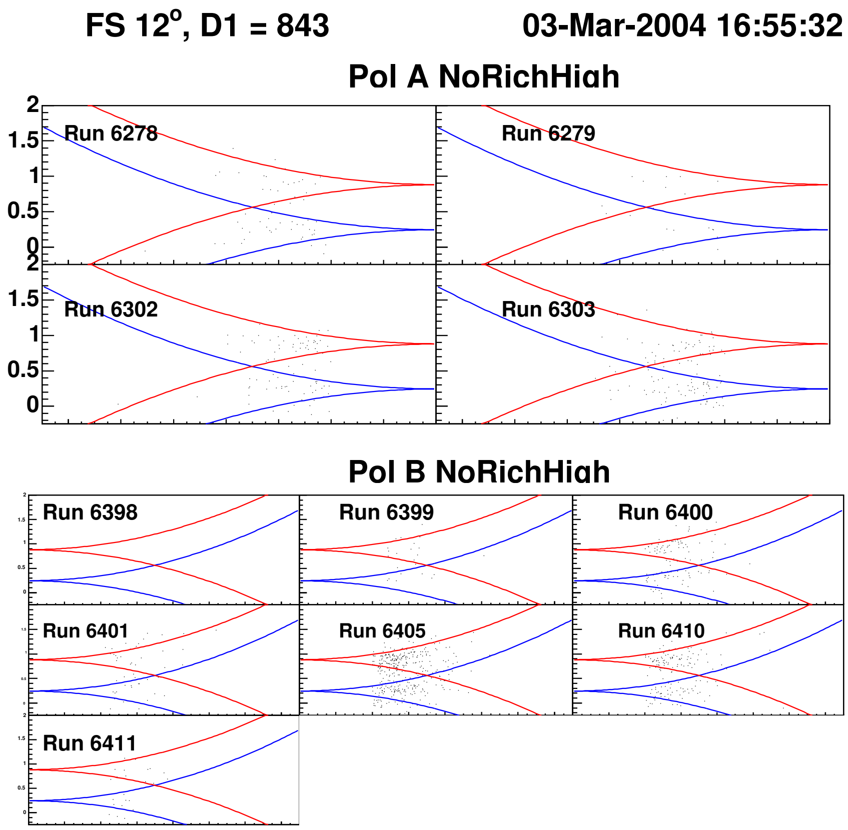

FIG. 32: 12^o BFS m^2 vs p (D1=843)

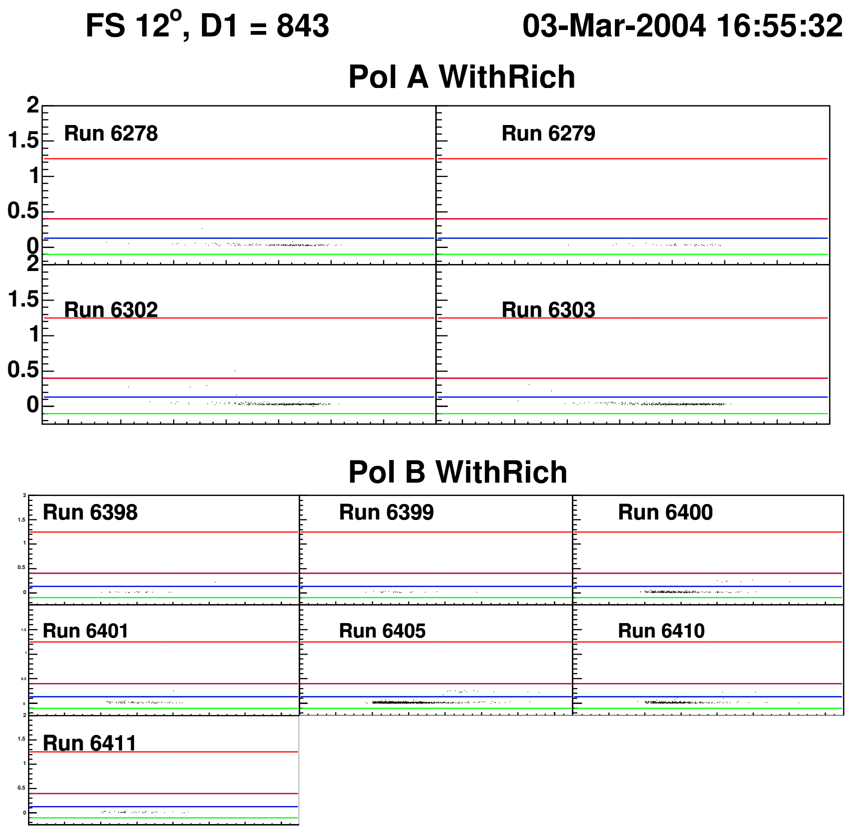

FIG. 33: 12^o BFS m^2 vs p (D1=843)

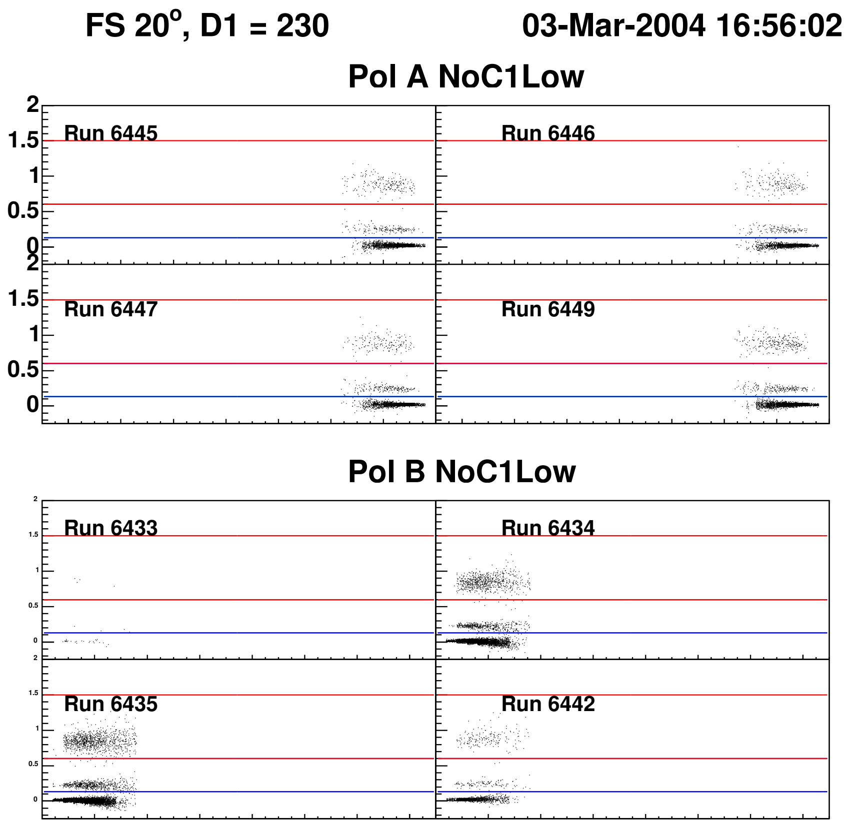

FIG. 34: 12^o FFS m^2 vs p (D1=843)

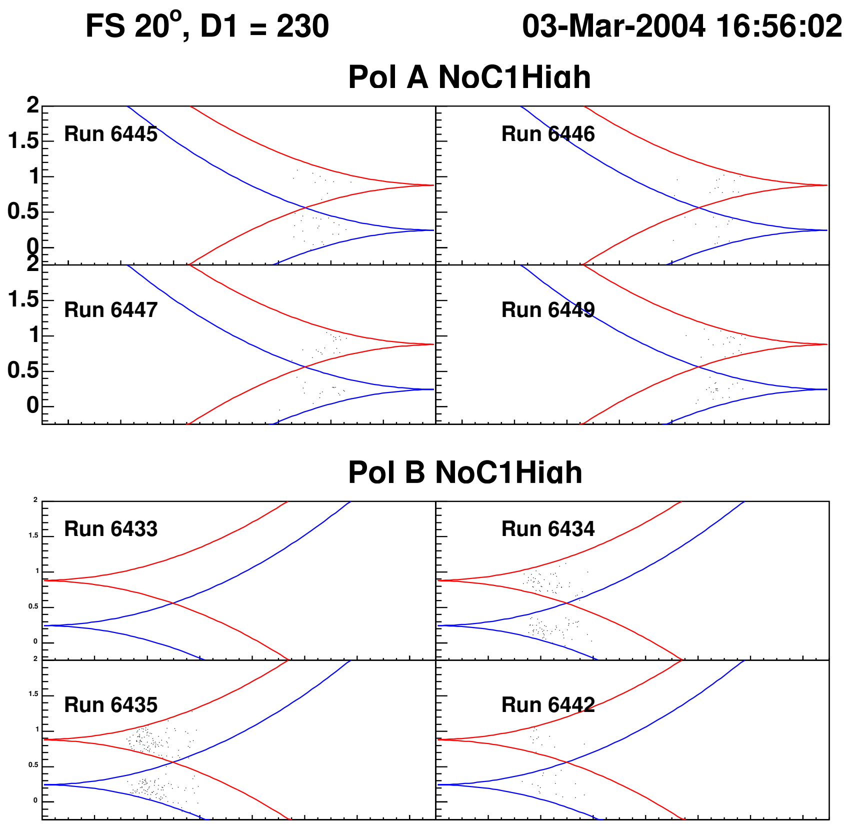

FIG. 35: 12^o BFS m^2 vs p (D1=843)

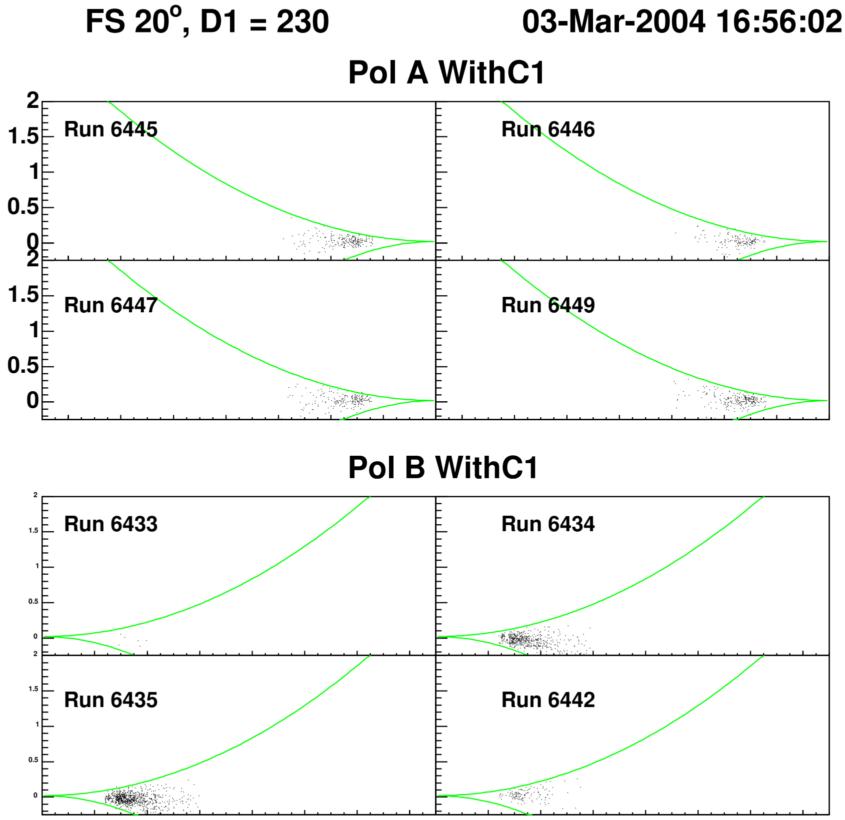

FIG. 36: 12^o BFS m^2 vs p (D1=843)

$\mathbf{p}_t$ spectra

Figure 43 shows the p_t spectra for the FS at the indicated angles when no gate is applied on rapidity. The solid symbols represent the points extracted from the BFS and the open symbols represent the points extracted for the FFS. Black represents positive particles and red represents negative particles. These are the different contributions coming from figures 16 through 18.

The FFS spectra were constructed by adding together the pid'd contributions from events where C1 did not fire and the particle had p less than the pion threshold (NoC1Low), where C1 did not fire and the particle had p greater than the pion threshold (NoC1High) and where C1 did fire (WithC1). In the same way the BFS spectra were constructed by adding together the pid'd contributions from events where RICH did not fire and the particle had p less than the pion threshold (NoRichLow), where RICH did not fire and the particle had p greater than the pion threshold (NoRichHigh) and where RICH did fire (WithRich). These are the different contributions coming from figures 19 through 21

Figure 44 shows the p_t spectra for the MRS at the indicated angles. There is no gate on rapidity applied to generate these spectra.

In figure 46 and 45 we show the p_t spectra for the MRS and FS, respectively, at the indicated angles. The rapidity gates for the various angles are shown in table V.

TABLE V: Rapidity windows used to construct ratios as function of p_t

angle	Spec	π	K	p
3	BFS	3.20-3.30	3.05-3.15	2.70-2.80
4	BFS	3.20-3.30	2.90-3.00	2.70-2.80
12	BFS	2.10-2.20	2.05-2.15	1.95-2.05
20	BFS	1.60-1.70	1.55-1.65	1.40-1.50
35	MRS	1.10-1.20	1.00-1.10	0.90-1.10
40	MRS	0.95-1.05	0.80-0.90	0.80-0.90
45	MRS	0.88-0.93	0.81-0.84	0.65-0.75
60	MRS	0.50-0.60	0.45-0.55	0.40-0.50
90	MRS	0.00-0.20	0.00-0.20	0.00-0.20

ratios

In this subsection we discuss preliminary results of the goal of the present analysis, namely the extraction of particle ratios. To start we examine the ratios as a function of p_t for the FS as well as the MRS.

The ratios as a function of p_t for the FS are shown in figure 47. There are no rapidity cuts applied to obtain

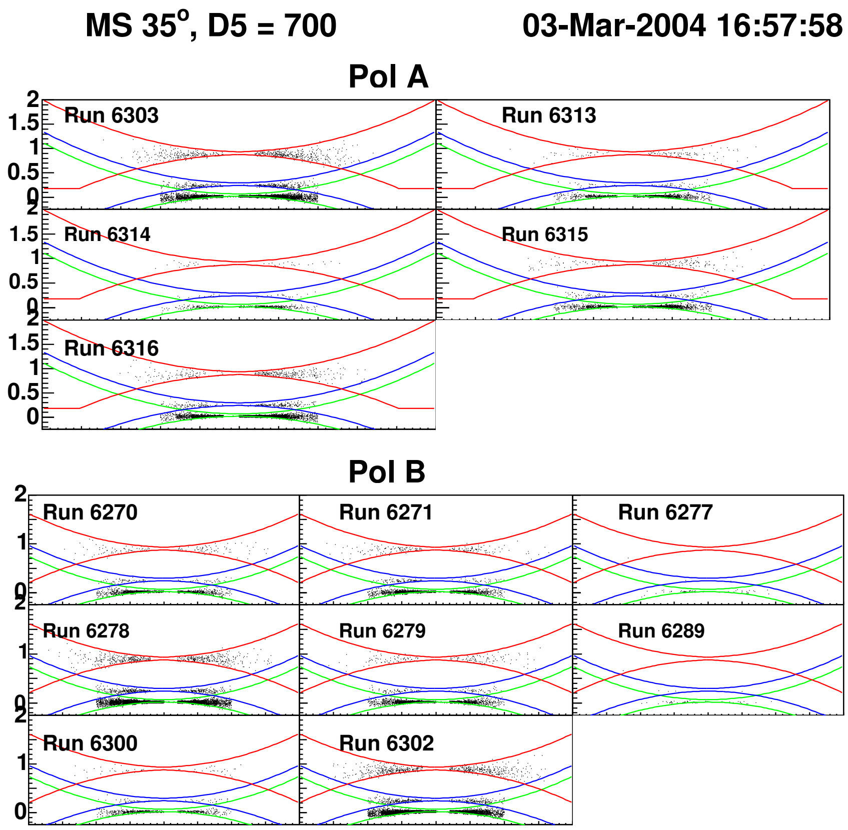

FIG. 37: 35^o MRS m^2 vs p (D5=700)

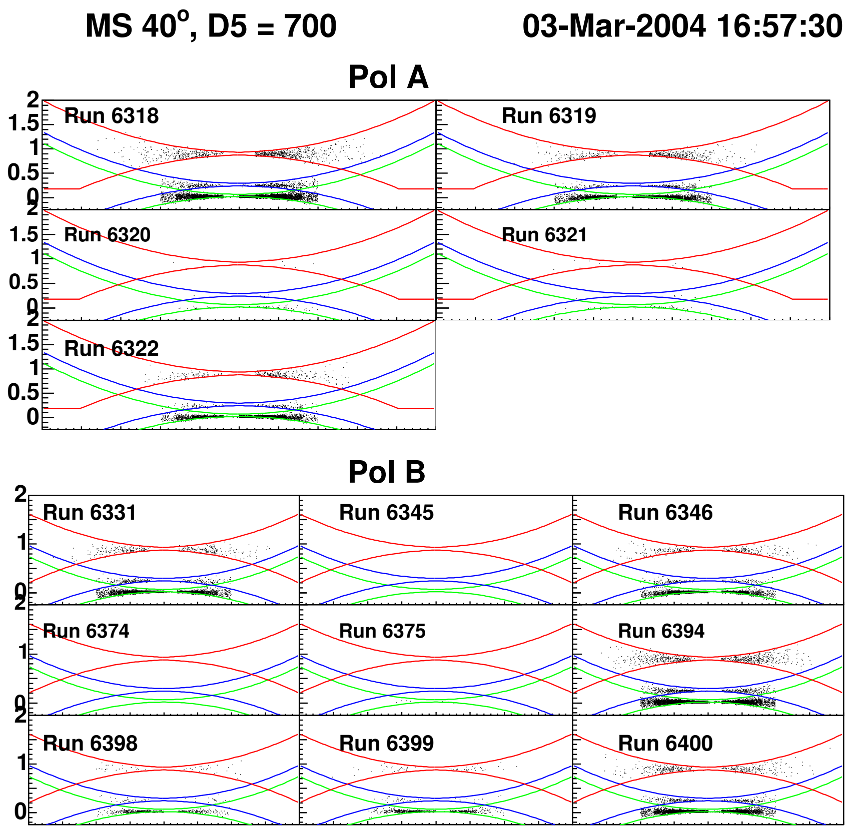

FIG. 38: 40^o MRS m^2 vs p (D5=700)

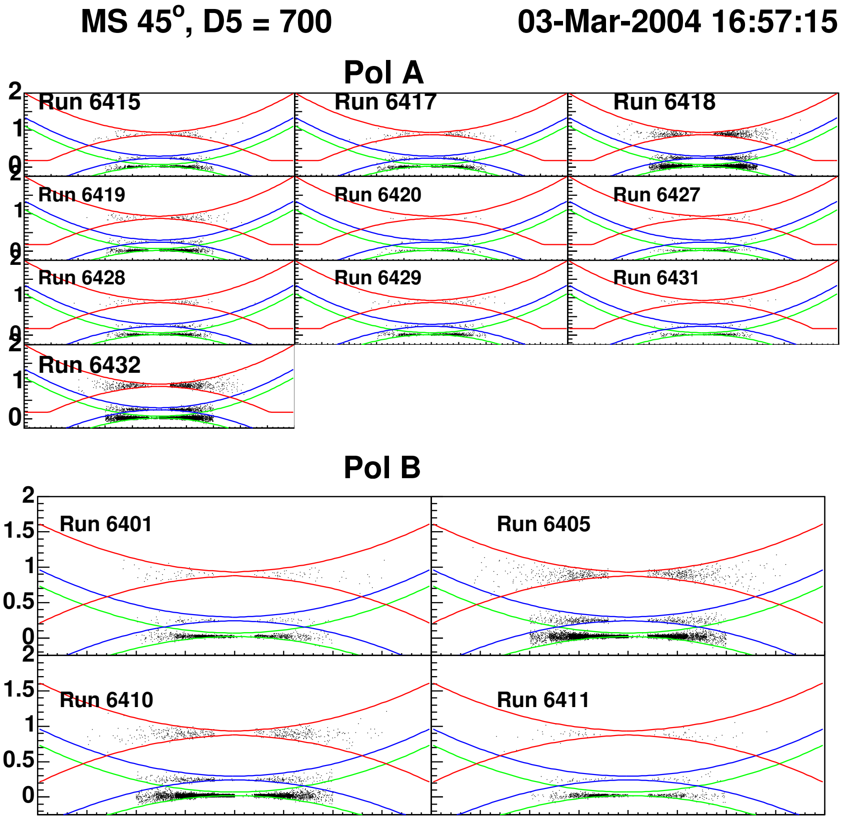

FIG. 39: 45^o MRS m^2 vs p (D5=700)

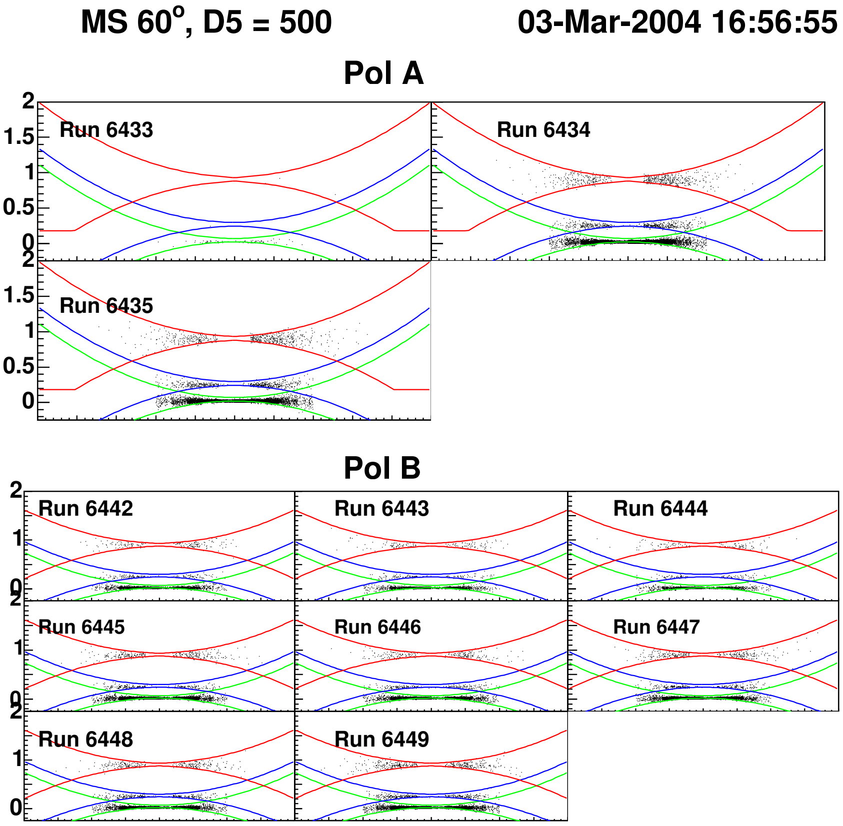

FIG. 40: 60^o MRS m^2 vs p (D5=500)

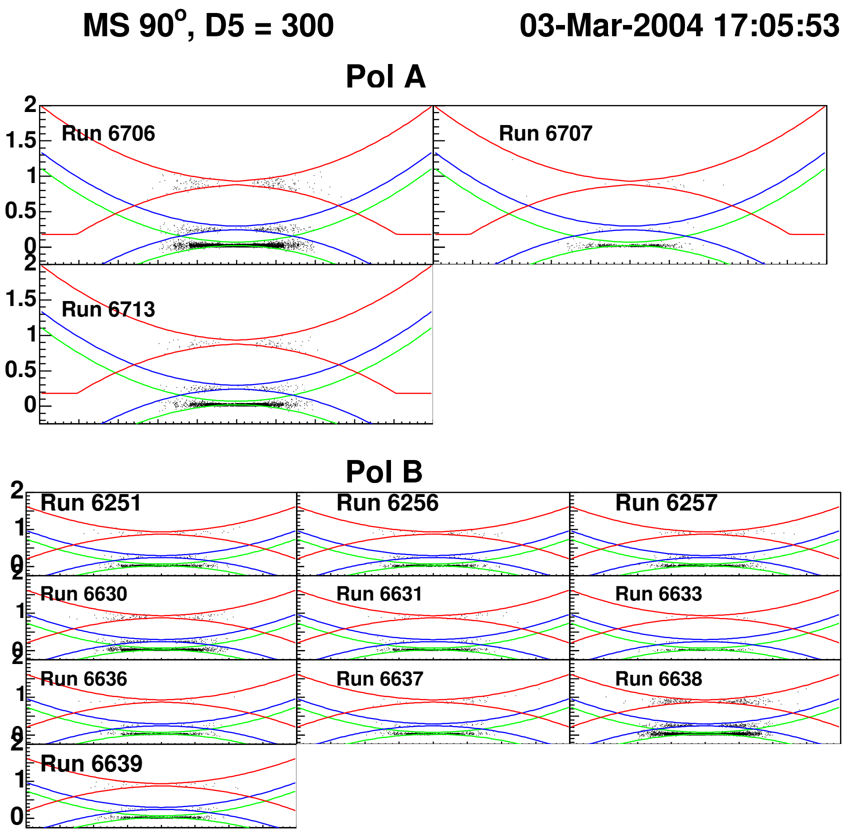

FIG. 41: 90^o MRS m^2 vs p (D5=350)

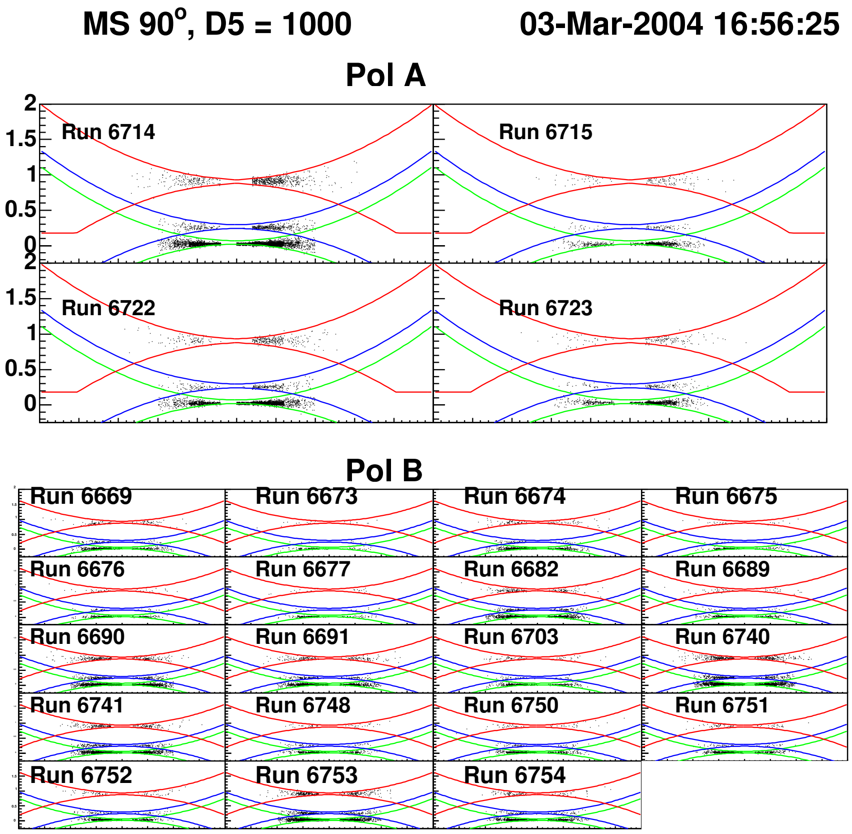

FIG. 42: 90^o MRS m^2 vs p (D5=1000)

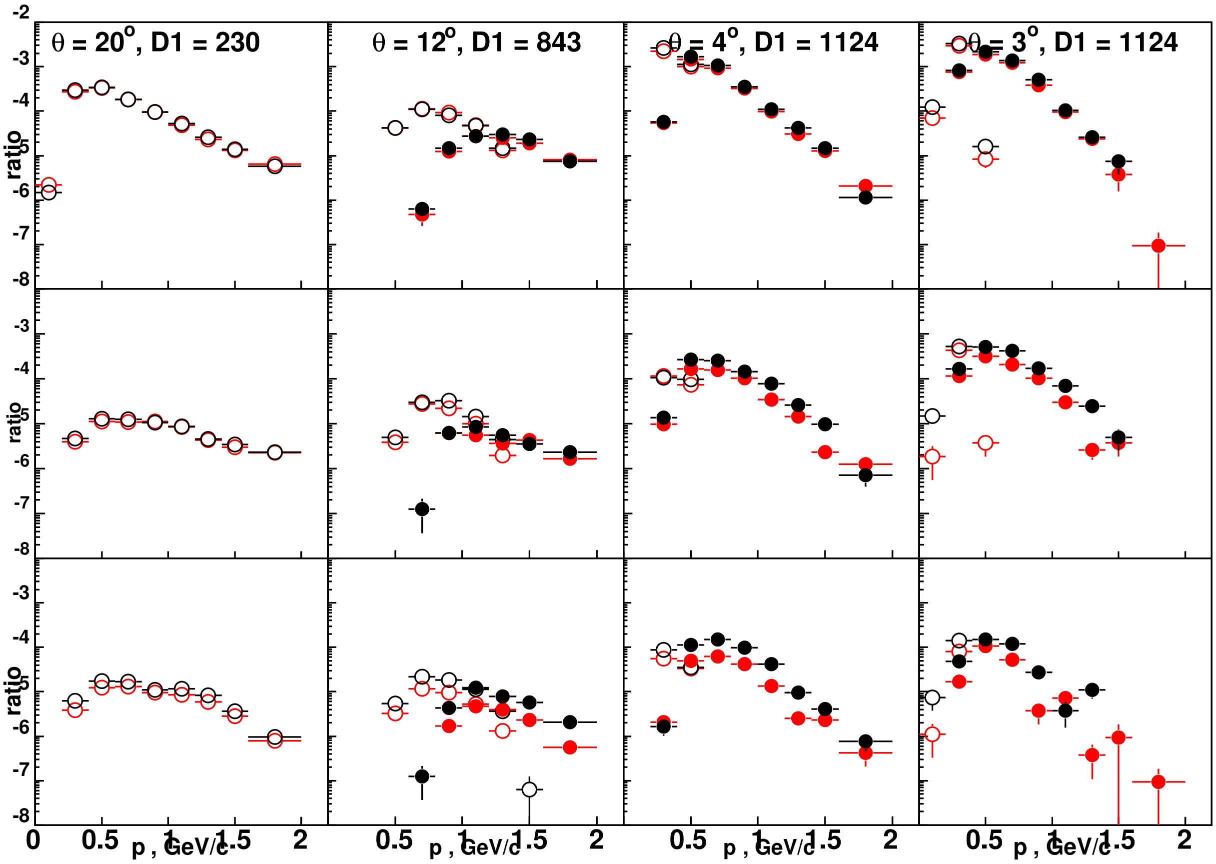

FIG. 43: p_t spectra in FS with no gate on rapidity

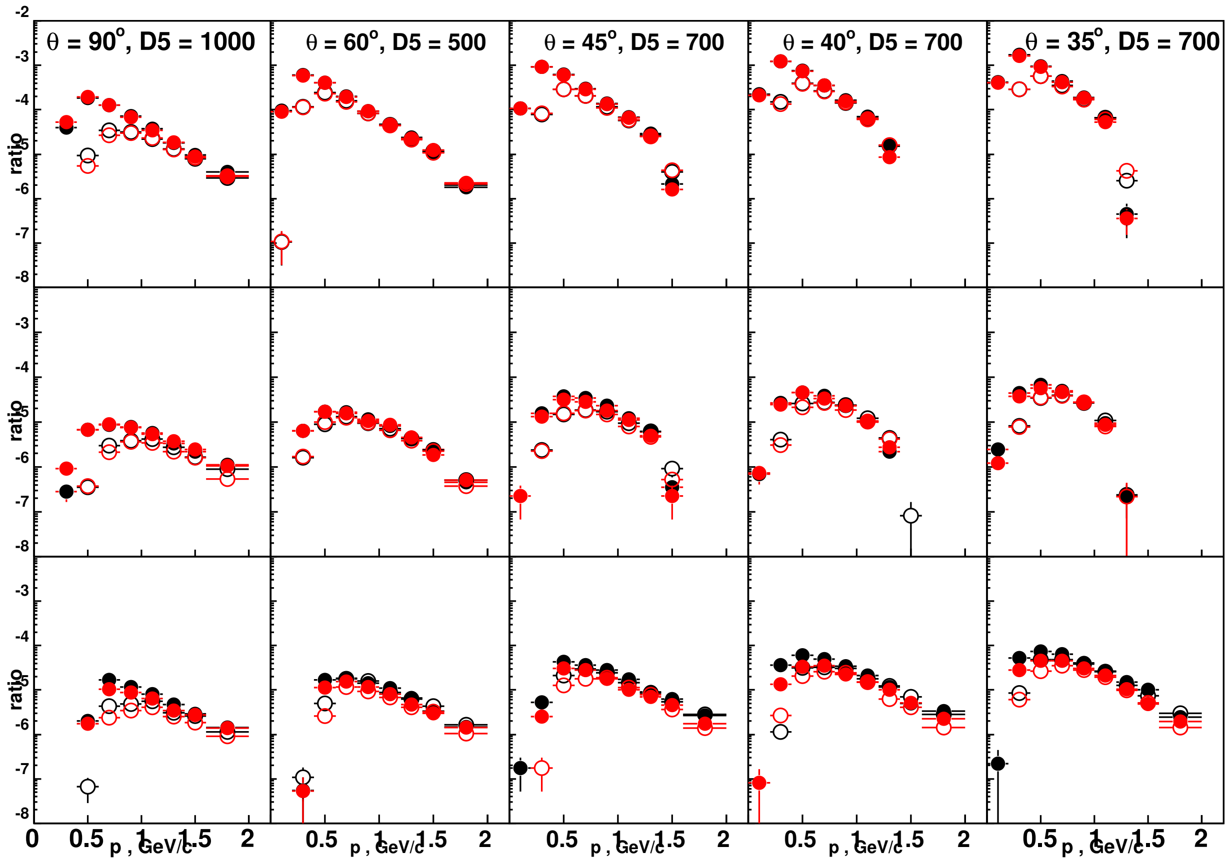

FIG. 44: p_t spectra in MRS for the indicated angles with no gate on rapidity

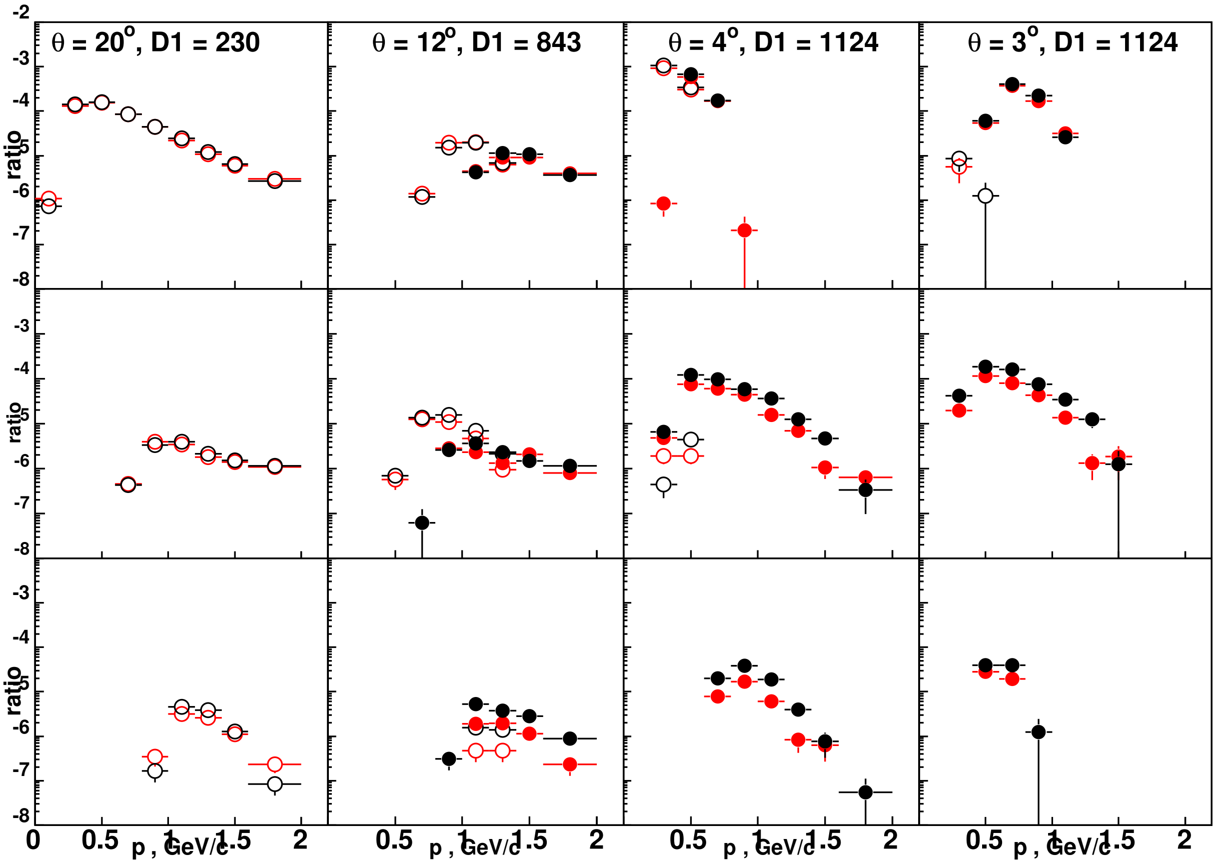

FIG. 45: p_t spectra in FS with gates on rapidity

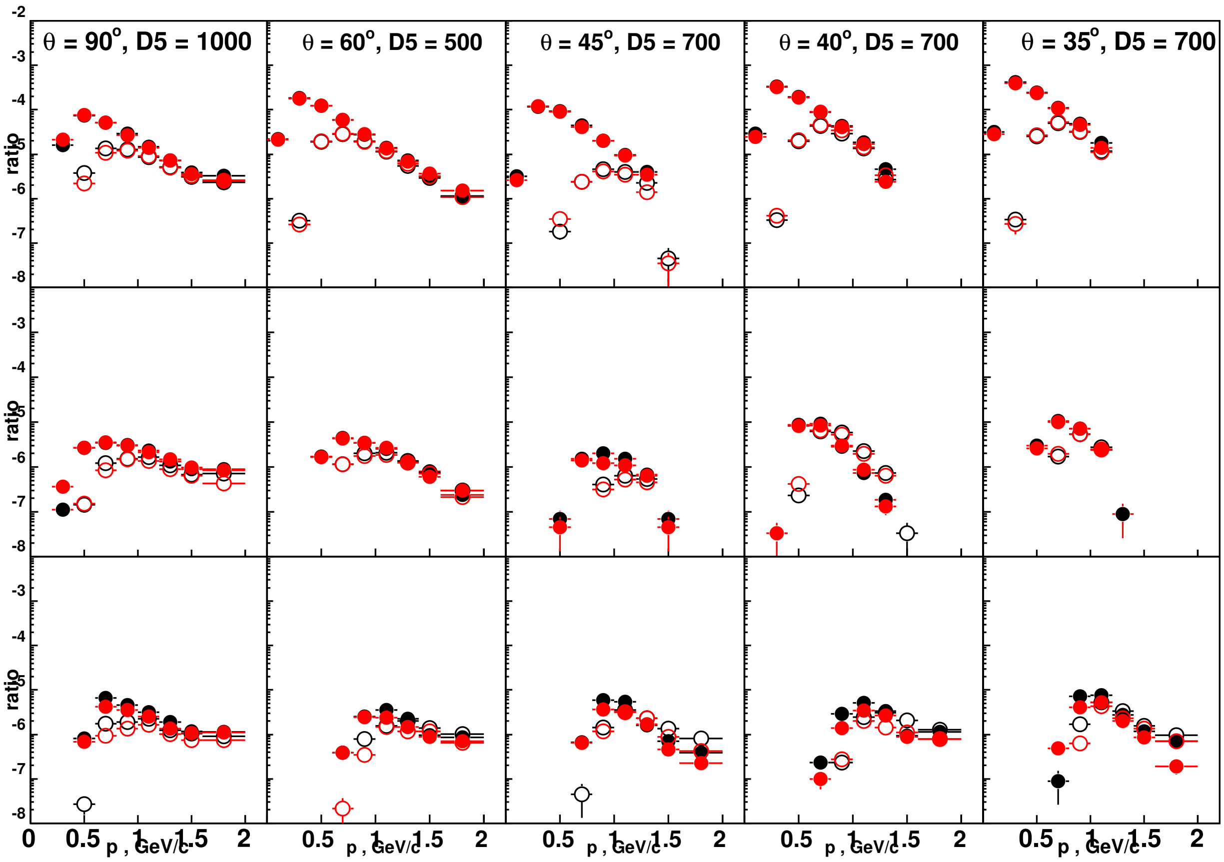

FIG. 46: p_t spectra in MRS for the indicated angles with gates on rapidity

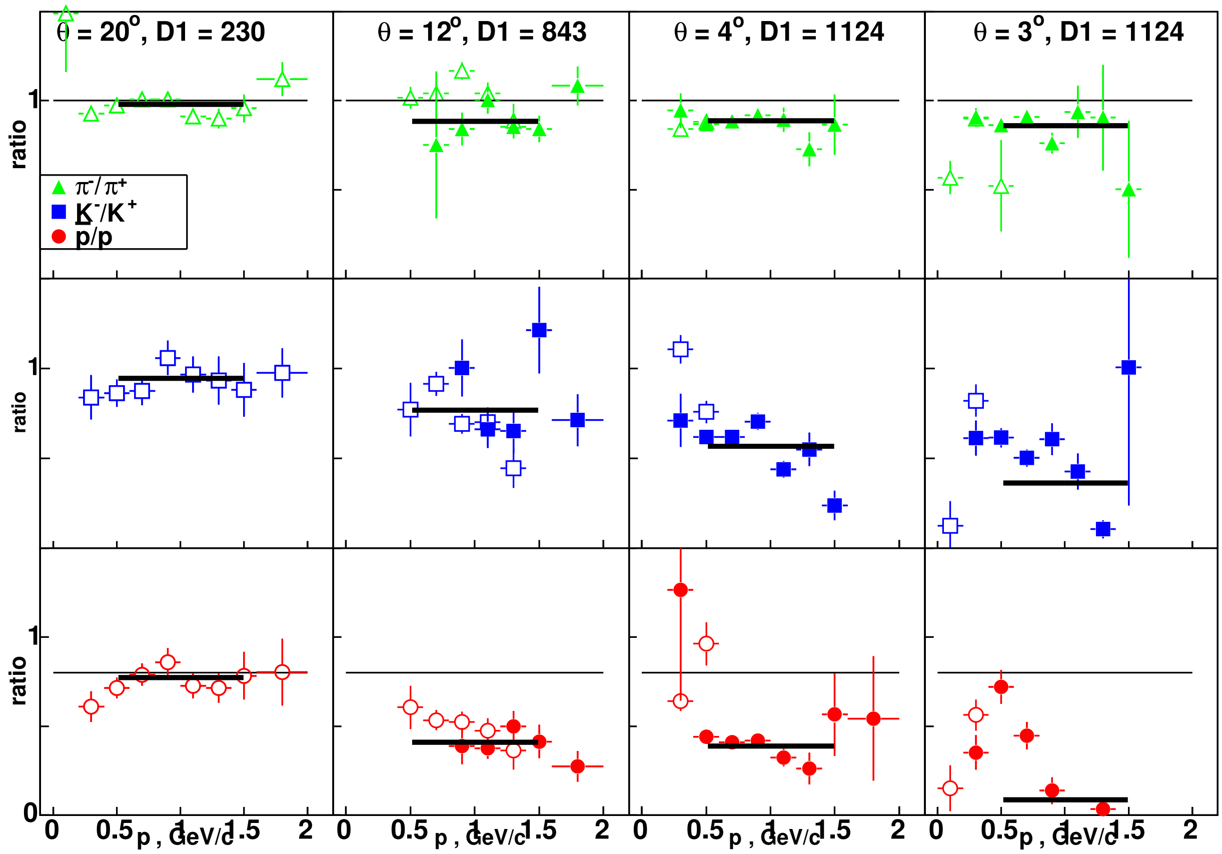

FIG. 47: p_t dependent ratios in the FS for the indicated angles and field settings obtained with no gate on rapidity. Open symbols indicate results from the FFS and closed symbols indicate results from the BFS

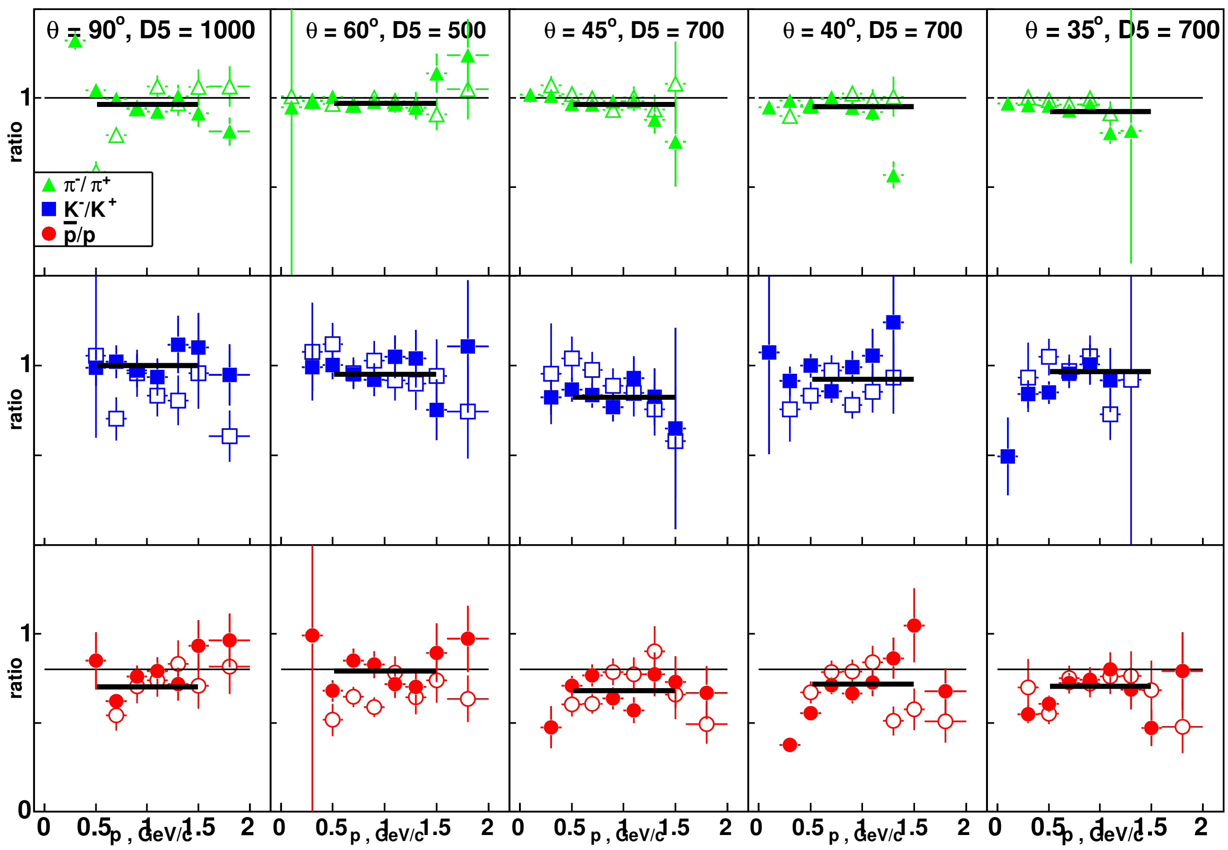

FIG. 48: Ratios in the MRS. No cuts in y are applied to these ratios

these distributions. These plots were obtained by dividing the positive and negative particle p_t spectra shown in figure 43. The open symbols show the results from the FFS and the closed symbols show the results from the BFS.

Shown in figure 48 are the ratios as a function of p_t for the larger angle settings, namely those of the MRS when placed at 35^o (D5=700), 40^o (D5=700), 45^o (D5=700), 60^o (D5=700), 90^o (D5=300) and 90^o (D5=1000), respectively. The full symbols represent the ratios calculated using the experimental normalizations.

Figures 49 and 50 show the ratios with the gates on rapidity shown in tableV. The lines show the results of a fit from p_t = 0.5 - 1.5 GeV/c. The results of those fits are shown in table VI. It is not clear why ratios in the 3^o setting are so different from those of the 4^o setting since they share the rapidity window.

One can see in figure 49 that the FFS and BFS ratios overlap within error bars in areas of overlapping p_t. In examining the forward data there appears not to be a p_t dependence on the ratios.

TABLE VI: Particle ratios integrated from p_t = 0.5-1.5 GeV/c

angle		Field	$\frac{\pi^-}{\pi^+}$	$\frac{K^-}{K^+}$	$\frac{\bar{p}}{p}$
3	BFS	1124	0.851 ± 0.0229	0.339 ± 0.0450	0.495 ± 0.1430
4	BFS	1124	0.958 ± 0.0550	0.560 ± 0.0335	0.372 ± 0.1030
12	BFS	843	0.844 ± 0.0685	0.738 ± 0.1030	0.407 ± 0.0642
20	FFS	843	0.978 ± 0.0229	0.939 ± 0.0860	0.700 ± 0.0757
35		700	0.941 ± 0.0188	0.956 ± 0.0561	0.645 ± 0.0428
40		700	0.956 ± 0.0156	0.958 ± 0.0537	0.631 ± 0.0400
45		700	0.943 ± 0.0218	0.732 ± 0.0677	0.639 ± 0.0390
60		500	0.987 ± 0.0130	0.973 ± 0.0408	0.750 ± 0.0385
90		1000	0.966 ± 0.0112	1.000 ± 0.0356	0.703 ± 0.0212

Another way to calculate ratios in the MRS is to use to our advantage that the MRS has acceptance for both positive and negative particles with a given polarity setting making a preferred acceptance for a given charge particle. Let $S_A(p_t)$ and $S_B(p_t)$ be the "true" p_t spectra for the A and B polarity settings, respectively. Furthermore, let $Y_A(p_t)$ and $Y_B(p_t)$ be the unnormalized p_t spectra. Then $S_A(p_t) = c_A Y_A(p_t)$ and $S_B(p_t) = c_B Y_B(p_t)$. If we take $S_{A_{pos}}(p_t)$ and $S_{A_{neg}}(p_t)$ to be the spectra of the positive and negative particles, respectively, accepted into the MRS for polarity A and likewise for polarity B, we obtain

$$R(p_t) = \frac{S_{B_{neg}}(p_t)}{S_{A_{pos}}(p_t)} = \frac{S_{A_{neg}}(p_t)}{S_{B_{pos}}(p_t)}$$

then

$$\frac{c_A Y_{A_{neg}}(p_t)}{c_B Y_{B_{pos}}(p_t)} = \frac{c_B Y_{B_{neg}}(p_t)}{c_A Y_{A_{pos}}(p_t)}$$

so that

$$\frac{c_B^2}{c_A^2} = \frac{Y_{A_{pos}}(p_t) Y_{A_{neg}}(p_t)}{Y_{B_{pos}}(p_t) Y_{B_{neg}}(p_t)} = f^2$$

Finally

$$R(p_t) = f \frac{Y_{B_{neg}}(p_t)}{Y_{A_{pos}}(p_t)}$$

A measure of how well the spectra are normalized using the normalization technique is to examine how near $\frac{c_B}{c_A}$ stays to 1 if the normalized spectra are treated as the unnormalized yield. The constants extracted when this is done are shown in table VII. We note that most of of the constants are within 10% of 1 indicating that the normalization extracted is probably good to within 10%.

The open symbols in figure 48 represent the ratios calculated using these cross ratios. They show the same trends as the ratios extracted using the formal normalizations, but are off by the percentage shown in table VII.

TABLE VII: Normalization constants obtained by comparing the normalized ratios with the cross ratios. A value of 1.0 indicates that the normalized ratios and the cross ratios agree.

angle	D5	pion	K	p
35	700	1.11	1.22	1.04
40	700	0.96	1.08	0.95
45	700	1.03	0.92	1.06
60	500	0.99	1.01	1.13
90	300	1.05	0.98	1.13
90	1000	1.10	0.97	1.08

If the p_t dependent ratios are fit over the range of $0.5 < p_t < 1.5$ GeV/c, we can obtain the rapidity dependent ratios. The results of the fits are shown as the thick horizontal bars in figures 49 and 50. The compilation of ratios extracted in this way is shown in figure 51.

SUMMARY

This analysis report has tried to present many details regarding the analysis of the p+p data of the 2002 run. The report is obviously a "work in progress".

Nevertheless we consider it a good idea to present the "status report" in order to have comment on any issues collaborators might have with analysis techniques. It is hoped that the results shown in this paper as well as the analysis report provided by Bjorn can be the basis of a paper on these interesting results.

[1] I. G. Bearden *et al.*, Phys. Rev. Lett. **90**, (2003) 102301.

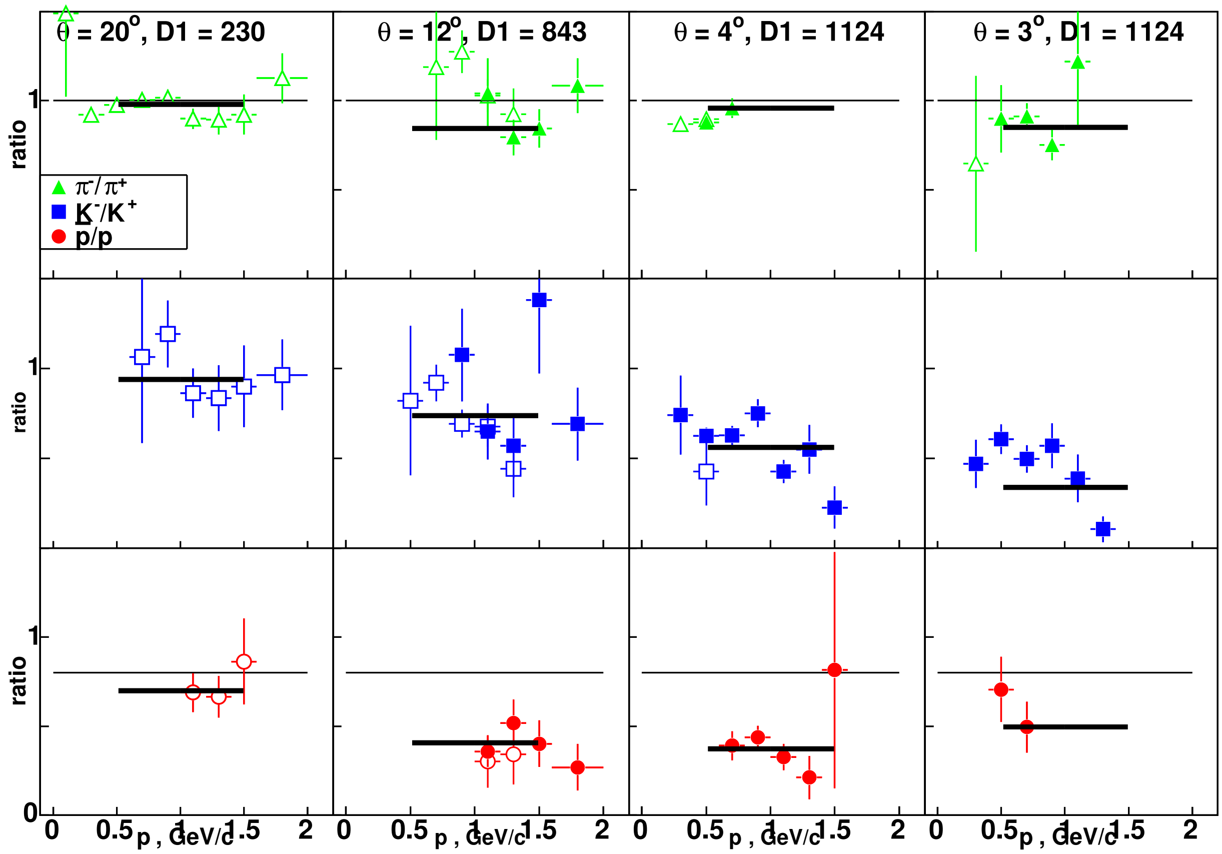

FIG. 49: p_t ratios in FS with gates on rapidity. The open symbols show the results from the FFS and the closed symbols show the results from the BFS. Note only open symbols in the 20^o setting because only the FFS was used at that angle

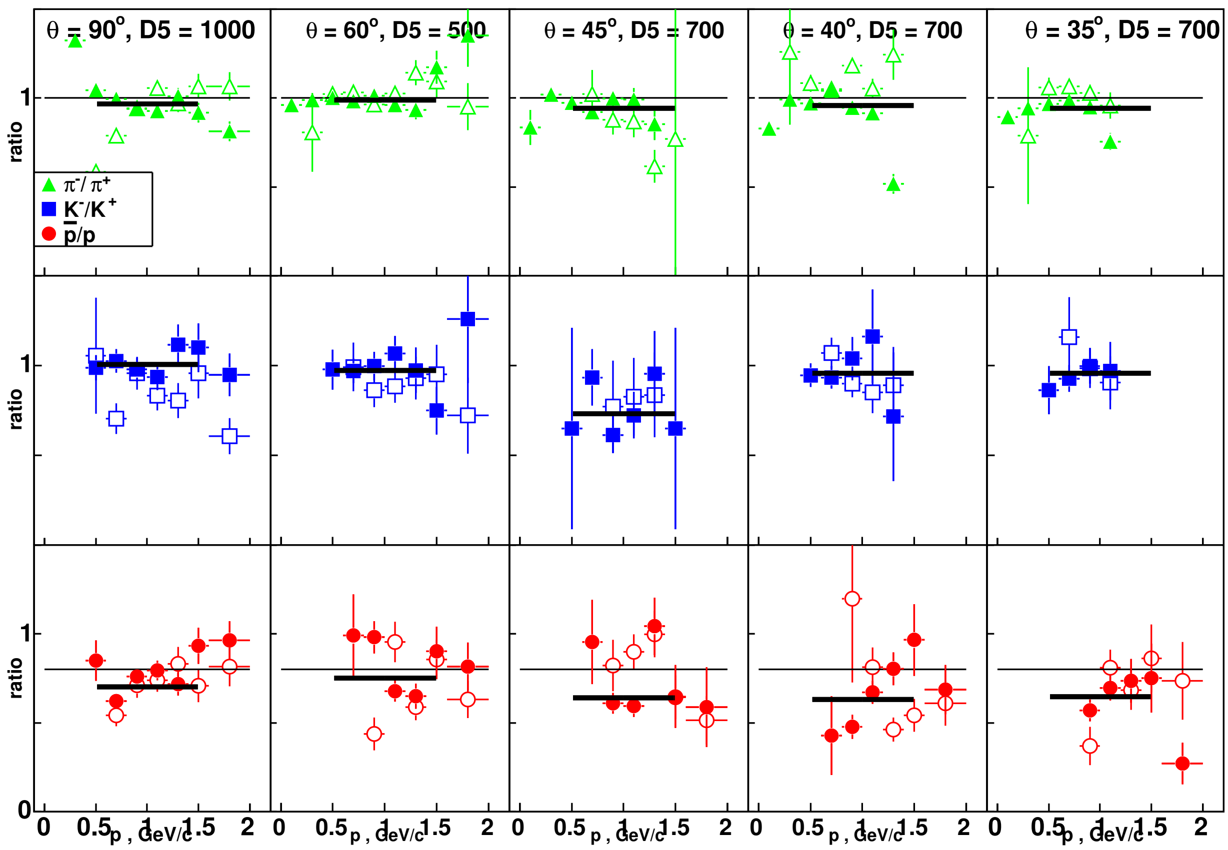

FIG. 50: p_t ratios in MRS for the indicated angles with gates on rapidity

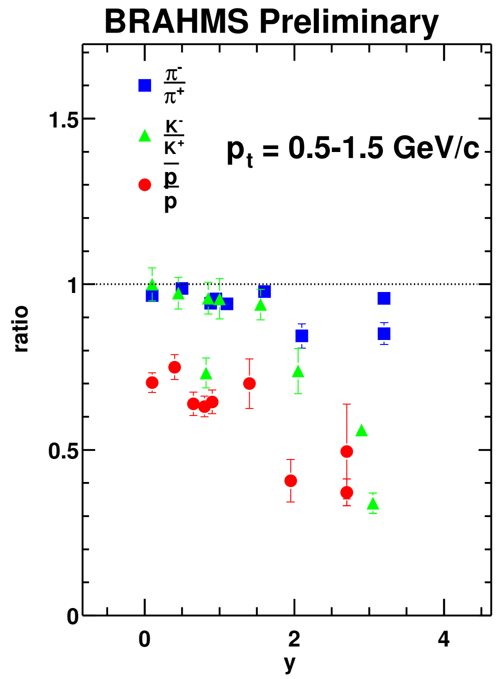

FIG. 51: Ratios of particles integrated in p_t from 0.5-1.5 GeV/c as a function of rapidity